TRIBHUVAN UNIVERSITY

INSTITUTE OF ENGINEERING

PULCHOWK CAMPUS

THESIS NO.: M-120-MSESPM-2018/2020

Flow analysis in eccentric bucket of Micro Pelton turbine: Multiphase modelling with transient state condition

by

Sourav Dhungana

A THESIS

SUBMITTED TO DEPARTMENT OF MECHANICAL AND AEROSPACE ENGINEERING IN PARTIAL FULFILLMENT OF THE REQUIREMENT FOR THE DEGREE OF MASTER OF SCIENCE IN

ENERGY SYSTEMS PLANNING AND MANAGEMENT

DEPARTMENT OF MECHANICAL AND AEROSPACE ENGINEERING

LALITPUR, NEPAL

JULY, 2020

COPYRIGHT

TRIBHUVAN UNIVERSITY

INSTITUTE OF ENGINEERING

PULCHOWK CAMPUS

DEPARTMENT OF MECHANICAL AND AEROSPACE ENGINEERING

The undersigned certify that they have read, and recommend to the Institute of Engineering for acceptance, a thesis entitled "**Flow analysis in eccentric bucket of Micro Pelton turbine: Multiphase modelling with transient state condition**" submitted by Sourav Dhungana in partial fulfillment of the requirements for the degree of Master in Energy Systems Planning and Management.

_____

Supervisor, Dr. Tri Ratna Bajracharya
Professor, Department of Mechanical and Aerospace Engineering, Pulchowk Campus

_____

External Examiner, Dr. Bhola Thapa
Professor, Department of Mechanical Engineering
Kathmandu University

_____

Committee Chairperson, Dr. Nawraj Bhattarai
Head, Department of Mechanical and Aerospace Engineering, Pulchowk Campus

Date: 31 July 2020

ABSTRACT

Micro hydro power plants use Pelton wheel to generate electrical power. Generally, bolted buckets are used in this type of power plants as it is small in capacity and size which makes easier to the operator to replace or repair old buckets whenever required. In this study, the effect caused by eccentricity of those bolted buckets on the operation of turbine is studied with the help of formulating mathematical model and conducting flow analysis in Computational Fluid Dynamics (CFD) code by ANSYS (CFX). Mathematical model has been developed to find the torque generated by eccentric bucket about three global axes, X, Y and Z. Torque has been obtained by calculating unbalanced forces in whirl and flow direction and compared with non-eccentric bucket condition to find the deviation. Numerical simulation has been carried out with outlet from nozzle maintained at constant 5.345×10^{-3} m^3/s flow rate to study the flow pattern in eccentric bucket and compared to that of non-eccentric bucket at five different angular positions showing velocity contour around the flow. The velocity distribution analysis revealed that the velocity is minimum at the bucket exit and maximum at the region near the splitter with values of 27.724 m/s, 28.688 m/s and 29.444 m/s for non-eccentric, 1° eccentric and 2° eccentric bucket respectively. Multiphase analysis at transient state condition has been conducted with complete 140 bucket rotation. The VOF scheme used for the multiphase analysis presented the deflection of water jet due to the eccentric splitter is increased with the increase in eccentricity. Torque has been monitored for single bucket and duplicated by using MATLAB software to obtain total torque generated. Maximum Pressure exerted on bucket has been obtained from numerical simulation and found to be 107.682 kPa, 125.765 kPa and 137.248 kPa at front side and 145.905 kPa, 160.059 kPa and 193.466 kPa at back side of non-eccentric, 1° eccentric and 2° eccentric bucket respectively. The pressure distribution analysis on back side of the bucket revealed that the maximum pressure occurred at 0 m from the splitter for non-eccentric condition and it goes increasing at 0.00378 m and 0.00599 m from the splitter for 1° and 2° eccentric condition respectively. The accuracy of the results was conformed by comparison of mathematical and numerical outputs by calculating the error. The error is found to be less than 6.017% in all non-eccentric, 1° eccentric and 2° eccentric buckets for torques generated about X, Y and Z-axis.

ACKNOWLEDGEMENTS

I would like to express my deepest gratitude and sincere thanks to my thesis supervisor Prof. Dr. Tri Ratna Bajracharya for his expert guidance, constant support and suggestion whenever required and continuous encouragement throughout the research period.

I would also like to express my sincere appreciation to the Department of Mechanical and Aerospace Engineering and Institute of Engineering for their support to the thesis. My appreciation extended to Dr. Nawraj Bhattarai, Head of Department of Mechanical and Aerospace Engineering, Pulchowk Campus for his co-operation and guidance. I would like to express my sincere gratitude and thanks to Associate Prof. Dr. Shree Raj Shakya, coordinator, MS-ESPM for providing a good interactive environment for thesis work and also to entire elite committee members for valuable comments and recommendation for making this work more meaningful. I would also like to thank Er. Ashesh Babu Timilsina and Er. Anil Sapkota for their valuable suggestions. I would also like to thank Er. Archana Ghimire, Er. Bikram Gaihre, Er. Ramesh Adhikari and all 074MSESPM colleagues for their constant support and suggestions.

I take this opportunity to extend sincere thanks and indebtedness to my family members for encouragement and the constant source of inspiration during the entire period of thesis work.

TABLE OF CONTENTS

LIST OF FIGURES

LIST OF TABLES

NOMENCLATURE OF SYMBOLS

OZ	:	Z-axis
P_1Q_1	:	Jet diameter (m)
PQ	:	Eccentric splitter
R	:	Pitch circle radius
x	:	Eccentric length CR (m)
r	:	Radius (CP) of the water jet (m)
PQRP	:	Area A_A (m^2)
PP_1ZQ_1Q	:	Area A_B (m^2)
$\overline{x}_A$	:	Centroid (CT) of Area A_A (m)
$\overline{x}_B$	:	Centroid (CS) of Area A_B (m)
α	:	Angle PCR (in radian)
δ	:	Angle of eccentricity ZOQ (in degree)
ρ	:	Density of water (kg/m^3)
a	:	Total jet area ($A_A + A_B$) (m^2)
v	:	Jet inlet velocity (m/s)
$v_{w_{in}}$	:	Bucket whirl velocity at inlet (m/s)
$v_{w_{out}}$	:	Bucket whirl velocity at outlet (m/s)
F	:	Force exerted by jet on bucket (N)
ϕ	:	Bucket outlet angle (Taken as $15°$)
u	:	Bucket peripheral velocity (m/s)
$v_{r_{in}}$	:	Relative velocity between bucket and water jet at inlet (m/s)
$v_{r_{out}}$	:	Relative velocity between bucket and water jet at outlet (m/s)
F_A	:	Force exerted by jet on area A_A (N)
F_B	:	Force exerted by jet on area A_B (N)
τ	:	Torque about splitter (Nm)
τ_x	:	Torque about X-axis (Nm)
τ_y	:	Torque about Y-axis (Nm)
τ_z	:	Torque about Z-axis (Nm)

LIST OF ACRONYMS AND ABBREVIATIONS

3D	:	Three Dimension
ANSYS	:	Analysis System
CFD	:	Computational Fluid Dynamics
CFX	:	CFD code by ANSYS
PCD	:	Pitch Circle Diameter
RPM	:	Revolution Per minute

CHAPTER ONE: INTRODUCTION

1.1 Background

Since 1911, a century has been passed, Nepal has been producing electricity from power generation stations under government and private owned companies (NEA, 2019). Francis and Pelton turbine are preferred in Nepal due to varied altitude ranging from mid hills to high hills. In Pelton turbine the flow enters and exits with tangent direction to the wheel and it is among the mostly used one globally (Rajput, 1998). They are measures for the generation of electricity which uses the hydraulic energy provided by the nozzle in kinetic form, which is converted to mechanical by the wheel and then into electricity later by the generator. Nowadays, efficiency as well as performance of the Pelton wheel has been improved tremendously due to development of modern technologies which helped to study behavior of fluids flow (Zhang, 2016).

Pelton turbine consist of buckets at the periphery of the center wheel where the water jet emerging from nozzle outlet strikes the wheel. The wheel uses the kinetic energy of water jet to generate mechanical energy. Finally, this energy is converted into electricity by the generator which is coupled to the shaft of the turbine. Whenever the geometrical parameters of Pelton wheel vary there is sharp decrease in the efficiency of the electrical energy generation.

More focused on distributed generation, nowadays, Micro Hydro Power has been used in huge number across the world due to small investment required and easy to maintain.

The electrical energy generated from the micro-hydro plant is green energy and is one of the most important renewable form of energy. Small sources of flowing water are extensively used to generate electricity. Small rivers and streams are very efficient sources for micro-hydro because they use run-of-river and they do not need large storage. The direct flow of water is entered into the turbine and then into the stream to generate the power. They almost do not contribute to environment deterioration and also considered as the most reliable and useful measure for generating electricity in the remote areas. (Gudukeya, 2017). Whenever there is availability of high heads, the use of Pelton wheel is preferred (Yadav, 2011). Firstly, while designing the Pelton wheel, empirical relations are used and then finally experimental analysis is done to obtain the final dimensions of the turbine (Avellan, et al., 2006). The turbine generates energy

from impulse action as water jet directly strikes the buckets which helps to rotate the center runner (Nasir, 2013). In this process the water jet contains energy only in the form of kinetic energy.

The components to be given most attention in Pelton turbine are nozzle and buckets. The buckets can be replaced easily if its profile is more distorted in the case of bolted buckets used by the small-scale Pelton hydropower. (Rainbow Micro Hydro, 2001)

To divide the water jet into two equal halves and reverse its direction, the shape of buckets as well as splitter plays a vital role. When this reverse action of jet occurs, impulse force is created due to Newton's Third law of motion by using kinetic energy of water jet. The design of buckets is done in such a symmetrical manner that the flow forces are cancelled and generation of axial forces is ceased (Eisenring, 1991).

Whenever the jet is coherent and at the correct speed, the problem is with the wheel. The mostly likely problem is that the jet is not hitting the wheel in the correct place which leads to sharp decrease in power as the jet moves outwards. It has been seen that this may lead to noise and vibration. (Thake, 2000)

1.2 Problem Statement

The bucket of Pelton turbine is the main portion where the water jet strikes to generate power. The efficiency of power generation in highly dependent on the profile of bucket. Large Pelton wheels are casted to form a single wheel. Whereas, in micro Pelton wheel the center wheel is manufactured and buckets are assembled with the help of nuts and bolts. On the process of assembling bucket, the planar alignment of splitter center line is not conformed due to mechanical processes applied. The purpose of splitter provided at the center of the bucket is to split water jet into two equal halves and then jet is diverted through 165° for the optimum generation of power. The splitter with wrong design and not well centered cannot break the jet into equal halves and thus reduces the efficiency. Moreover, to decrease in efficiency, the physical difficulties such as vibration due to force unbalance and uneven erosion on both side of splitter occurs frequently. The problem in such bucket with eccentric splitter is the uneven pressure and force distribution.

The eccentric angle is measured between original and displaced splitter position as shown in Figure 1.1. This research will provide basic idea about the effect of such eccentric bucket.

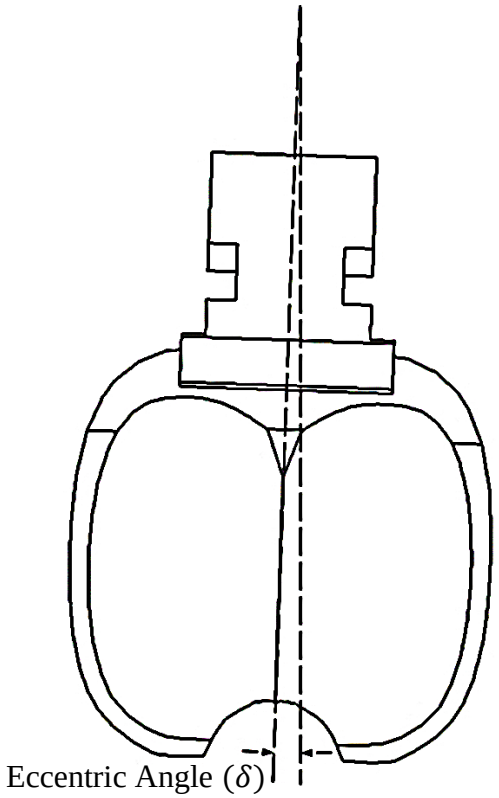

Figure 1.1: Bucket with eccentricity

1.3 Rationale of the Study

This study will analyze the effect of Pelton bucket splitter eccentricity change to the efficiency and power output. Such type of analysis will be helpful for the design consideration for the companies and for the repair and maintenance of the turbine in micro hydropower projects. Pelton Bucket splitter eccentricity will lead to uneven dividing of the jet flow which will lead to the vibration of the turbine and causes the decrease in efficiency as well as may also cause shutdown of the plant which may cause huge economic losses to the project. These losses can be minimized. This study will also help to minimize the effects caused by eccentricity of the splitter of the Pelton and increasing the reliability of the plant. Hence, the performance of the plant can be improved.

1.4 Objectives

1.4.1 Main Objective

The main objective of this thesis is to perform transient flow analysis in eccentric bucket of micro Pelton turbine with multiphase modeling.

1.4.2 Specific Objectives

The specific objectives for the study of eccentric bucket are,

- To mathematically model the torque generated by eccentric bucket.
- To conduct the flow analysis in computational platform.
- To study the distribution of pressure exerted by water in the bucket.
- To compare the results obtained from numerical analysis with mathematical model.

1.5 Assumptions and Limitations

- CFD analysis is done by considering three buckets.
- Water is considered as incompressible fluid.
- Heat transfer between buckets and water due to friction is neglected.
- Structural deformation of buckets is not considered.
- Casing covering the Pelton wheel is not considered.

CHAPTER TWO: LITERATURE REVIEW

2.1 The Pelton turbine

A Pelton wheel consists of center wheel in which double hemispherical buckets are attached at the periphery with equally spacing between them. Penstock carries water from a high head storage or reservoir to the power house and nozzle converts it into high speed jet at the outlet. The water flow is controlled by the needle spear in a smooth manner with a minimum energy loss at the nozzle. All the potential energy of the water coming out of nozzle is completely converted into kinetic energy just before hitting the buckets by the action of nozzle and spear needle. Since, Pelton wheel is subjected to atmospheric pressure fully, there is no chance of pressure difference between any two sections of the turbine. Hence, the energy transfer is completely due to impulse action only between jet and bucket.

Splashing of water is prevented by casing which is provided to cover the Pelton wheel and to guide water towards the tail race. Whenever there is necessity to discontinue the rotating of Pelton wheel, spear needle is moved forward to fully close the opening of nozzle. A brake nozzle is also provided in Pelton turbines whose purpose is to bring Pelton wheel, rotating due to inertia, to rest after the cease of jet due to complete closing of nozzle with the help of spear needle, by hitting at the back of the buckets by secondary jet known as braking jet.

At the center of the bucket, a splitter is provided whose sole purpose is to divide the water jet into two equal halves and assist dividing force exerted by water equally. Since water jet tends to carry sand particles and other abrasive materials, which cause erosion and wear in the bucket inner surface and splitter, splitter is generally avoided to form a mathematical cusp. Manufacturing difficulties is also another major cause which avoids the formation of mathematical cusp for line at the center of bucket.

Theoretically, for maximum power generation, the relative velocity of jet leaving the bucket must be exactly opposite in direction to the relative velocity of jet at entering condition but in real in it not possible due to interference between two jets and jet and incoming bucket back. So, it is practiced to keep the angle of leaving jet close to 180° as much as possible. In real cases, it is almost kept at 165° to 170° for all buckets worldwide which makes the shape of bucket slightly smaller than a hemisphere. This

arrangement of jet leaving angle reduces the back-splashing of jet to incoming bucket back and also helps to maintain turbine efficiency in an optimum manner.

The geometry of Pelton bucket is shown in Figure 2.1.

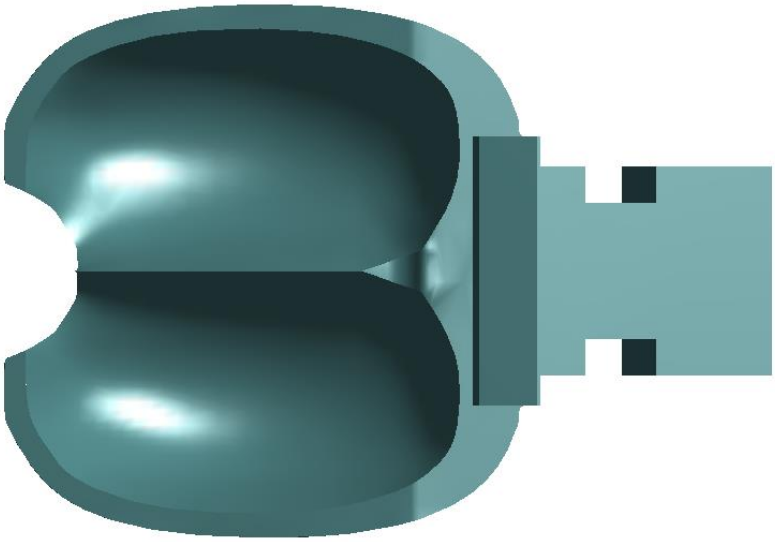

Figure 2.1: Top view of Pelton Bucket

2.2 Energy conversion

The energy in the Pelton turbine, before jet strikes the bucket, is totally changed into kinetic form by the nozzle, which makes it absolute impulse action turbine. Since, runner is fully exposed to atmosphere, the pressure between the inlet and outlet is same, restricting the runner to generate energy due to pressure difference (Sangal, et al., 2013). The shaft carries the mechanically generated energy by runner to the generator, which is solely effect of impulsive forces. Whenever the shape of buckets guides the flow of jet to change its direction, impulse force is generated according to Newton's Second Law of motion.

Figure 2.2 shows the conversion of energy from inlet of needle to the outlet of wheel at Pelton turbine in a graphical form with respective parameters and variables mentioned (Brekke, 2001). The energy conversion in the flow at nozzle starting from needle inlet to needle outlet is represented by Step 1-2. In this step, the final state of water is exposed to atmospheric pressure with high velocity, initiating from the initial state of slow moving highly pressurized water. At outlet the energy possessed by water jet is completely kinetic. The following Step 2-3 starts from the nozzle outlet and the kinetic energy carried by water jet is utilized by the runner to generate mechanical energy. The

energy transfer between jet and the Pelton wheel can be expressed in the form of Euler's Head H_e using the variables peripheral velocity and whirl velocity of the runner taken at the inlet and outlet conditions (Bansal, 2010) as shown by Equation 2.1.

$$H_e = \frac{V_{w_1}u_1 - V_{w_2}u_2}{g} \qquad \text{Equation 2.1}$$

where V_{wi} and u_i is the whirl and peripheral velocity respectively.

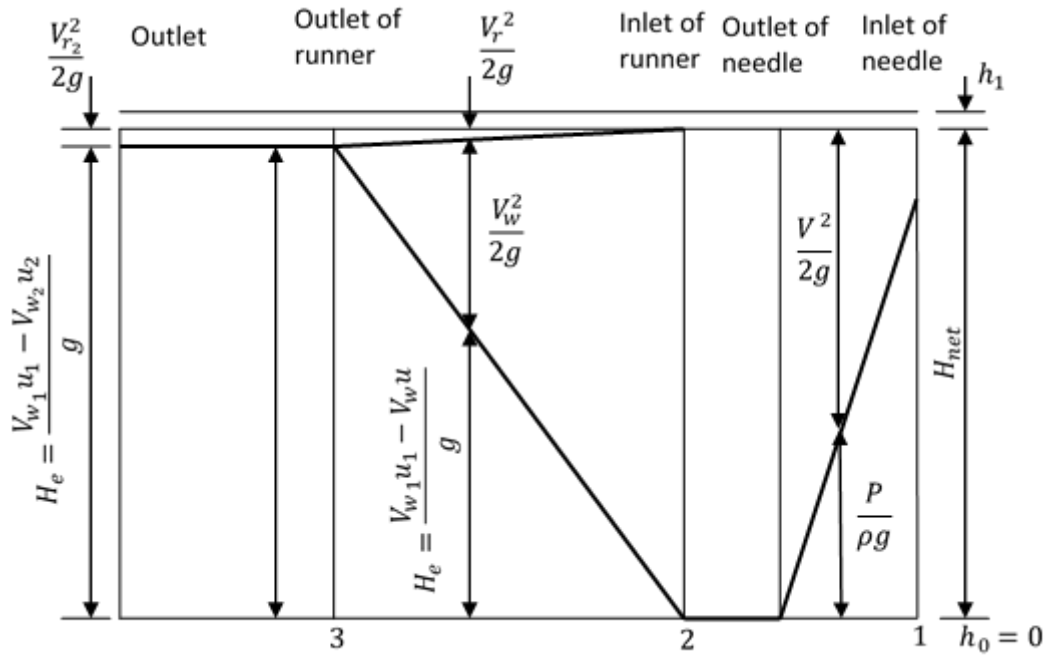

Figure 2.2: Process of energy conversion from inlet of nozzle to outlet of runner in a Pelton turbine

In step 2, the remaining energy can be divided into two components: (1) a small flow velocity $\frac{V_{r_2}^2}{2}$ (relative to the jet) and (2) the potential energy gh_1 of the water relative to the tail-water.

2.3 Maximum Water Jet Velocity

The Bernoulli equation given by Equation 2.2 (White, 2008) when expressed for a streamline in a flow which is incompressible, steady, frictionless and irrotational is

$$\frac{p_2 - p_1}{\rho} + \frac{v_2^2 - v_1^2}{2} + g(h_2 - h_1) = 0 \qquad \text{Equation 2.2}$$

The conservation of energy can be achieved between any two points in a streamline whenever other losses are not taken into consideration. Equation 2.2 can be taken and re arranged to solve for v_1, to get the final expression for actual jet velocity.

$$v_{1,max} = C_v\sqrt{2gH_e} \qquad \text{Equation 2.3}$$

The losses are not considered in Equation 2.2, which plays a major role in determining the characteristics of jet. So, a coefficient C_v to account for the flow losses such as friction is defined and finally incorporated in Equation 2.3 (Kjølle, 2001).

2.4 Study on Bucket and Flow

The major extensive study on splitter is focused on the erosion and width change of the splitter which in turn assists in declining efficiency and vibration of the wheel. The major researches conducted in the related topic which are useful for study of bucket eccentricity are:

Panthee, Thapa, & Neupane, 2014 conducted the flow analysis showing that three buckets are sufficient to analyze the power generated by the Pelton wheel.

Batbeleg & Lee, 2018 have shown the calculation involved in finding power using rpm and torque generated from the numerical simulation which can be compared to installed capacity which helps for a micro Pelton turbine to evaluate the efficiency.

Solemslie & Dahlhaug, 2015 have shown the comparison of bucket load with specific speed. The variation of bucket loads was plotted with varying specific speeds of the Pelton wheel.

In 2014, Chukwuneke et. al. has performed a study to present the relation between head splitter angle and head and the generation of the turbine.

In 2017, Christian et. al. presented a technique based on the geometry of the bucket with parametric analysis which used the computational platform and modern optimization techniques to minimize the geometrical dimension of the problem to be designed.

2.5 Computational Fluid Dynamics (CFD)

Whenever, the fluid problems are too difficult to solve by analytical method, Computational Fluid Dynamics (CFD) plays important role by applying computational

methods to obtain fluid flow patterns and solution of problems. Nowadays, CFD is becoming a powerful tool because of rapid growth in scientific technology and availability of high-end computers with strong specifications. Solving procedures for Navier-Stokes equations in theoretical conditions is an easier process but whenever situation occurs for obtaining solution to real problems a computational method is preferred in which all the constraints are approximated by the general algebraic expressions and it is later solved in an iterative way for smaller areas to obtain final results for actual problem.

2.5.1 Turbulence Modelling

The flow which follows a predefined streamline throughout the analysis for a specific time period, it is known as laminar flow. When in that certain flow the parameter values starts to increase and it attains highly disturbed flow regime throughout the analysis time, it is known as turbulent flow (Riveros & Riveros-Rosas, 2010).. Turbulent flow is highly irregular and non-linear with high dissipation of energy and diffusivity forming vortex. Whenever a study of highly turbulent flow is required, it is followed by a rigorous approach with involvement of complex parameters and processes.

Laminar and turbulent flow is characterized by the study of Reynold's Number, which is defined as the ratio of inertial force to the viscous force. Whenever its value is higher, that means inertial force overcomes the viscous force disturbances and disorder occurs known as turbulence. Reynold's Number is defined mathematically as,

$$Reynold'sNumber\ (R_e) = \frac{Inertial\ Force}{Viscous\ Force} = \frac{VL}{\nu} \qquad \text{Equation 2.4}$$

Where, V, L and ν represents the velocity, length and kinematic viscosity of fluid.

In real field, all the fluid flow which are to be studied in an engineering design or research are almost turbulent (Eggenspieler, 2012). Among several techniques for solving the turbulence model, Direct Numerical Simulation (DNS) numerically solves the governing equation of the fluid flow: Navier-Stokes equations. It does not require any model and has high computational cost. Scale Resolving Simulation (SRS) which includes Large Eddy Simulation (LES) resolves the motion of largest eddies in the calculation and smaller eddies than the mesh is modeled. It is an inherently unsteady method as it generates long run times and large volume data due to small time steps and

requires higher grid resolution. Reynolds Averaged Navier-Stokes Simulations (RANS) is most used and appropriate approach for Pelton turbine simulations. DNS and SRS are more demanding and complex for the problem herein.

Reynolds Averaged Navier-Stokes (RANS)

RANS model solves the Reynolds averaged Navier-Stokes equations in a time averaged framework in which steady state solution are possible. It models all turbulence including the large eddies. For the analysis of flows in an industrial application, it plays a vital role and it is also extensively used for conduction analysis of turbulent flow with steady state approach. To represent the highly turbulent fluctuations mean value of the flow quantities are used by the equations in this approach. It is also called Statistical Turbulence Model due to its nature of using statistical averaging procedure.

SST Model

Originally, k-ω was developed to conduct analysis for near wall problems so it has some difficulties while conducting free stream problems. So, to overcome this situation, a combination between k-ε model at the free stream region and k-ω model ant the near wall region was developed (Menter, 1994). This model was named as Shear stress Transport (SST) model and it used two different steps in which a blending function and its compliment is multiplied with k-ω and transformed Launder-Spalding k-ε model equations respectively.

The model has more advantages and provides more correctly predicted outputs for the flow conditions with turbulent shear stress and as well as to represent the flow separation under high gradients of pressure as it adds the benefits of both Launder-Spalding k-ε and Wilcox k-ω model in an very effective way.

2.5.2 Multiphase Modeling

Multiphase flow consists of more than one fluid for example, water and air in the Pelton turbine (Nigussie, et al., 2017). Whenever the water leaves the bucket it becomes dispersed and gets mixed with air. This makes the flow in Pelton turbine to be multiphase. Continuous phase can be approximated for the multiphase flows which contains tiny particles and droplets to conduct the simulation for achieving the required outputs and results.

Whenever this multiphase flow disperses more, there occurs difficulties to obtain the results from computational analysis. Due to development of modern computerized technology with powerful specification, the hardware is less considered as the hindrance for the simulation rather the availability of equations which models the turbulent flow accurately is a major problem nowadays. However, actual common processes involve combination of different multiphase, multiphase flow are considered one of the important as well as challenging analysis in engineering.

Volume of fraction (VOF)

One of the parameters that are used to characterize multiphase flows is the volume fraction, which is the actual volume of a single phase in a specified sub region divided by the total volume and it is taken as the most prominent parameter (Xiao, et al., 2012). The volume fraction for a phase in a unit volume of the cell is the actual volume occupied by the phase occupied in that particular cell.,

$$\alpha_1 = \frac{\sum_{n=0}^{N} V_n}{V} \qquad \text{Equation 2.5}$$

where α_1 is the volume fraction of fluid 1, V_n is the volume occupied by particle of fluid 1 and N is the total amount of particles of a phase present in total volume V. Now, the volume fraction of fluid 2 (α_2) can be calculated by,

$$\alpha_2 = 1 - \alpha_1 \qquad \text{Equation 2.6}$$

CHAPTER THREE: METHODOLOGY

This chapter describes the methodology that is opted to apply for the work from start of the project till the completion. The flow diagram of methodology followed during the process of project is shown in Figure 3.1. Literature review is followed by two procedures. At one side mathematical modelling is done which consists of identification of variables and parameters, development of mathematical model and finally its solution. Similarly, at other side, flow analysis is conducted which consists of CAD modelling of geometry, physics setup and simulation and finally its solution with post processing. These two steps are repeated for three conditions: non-eccentric, 1° eccentric and 2° eccentric bucket. The results from mathematical and simulation analysis are compared. Finally, presentation and documentation of the study is done after critical discussion of the results.

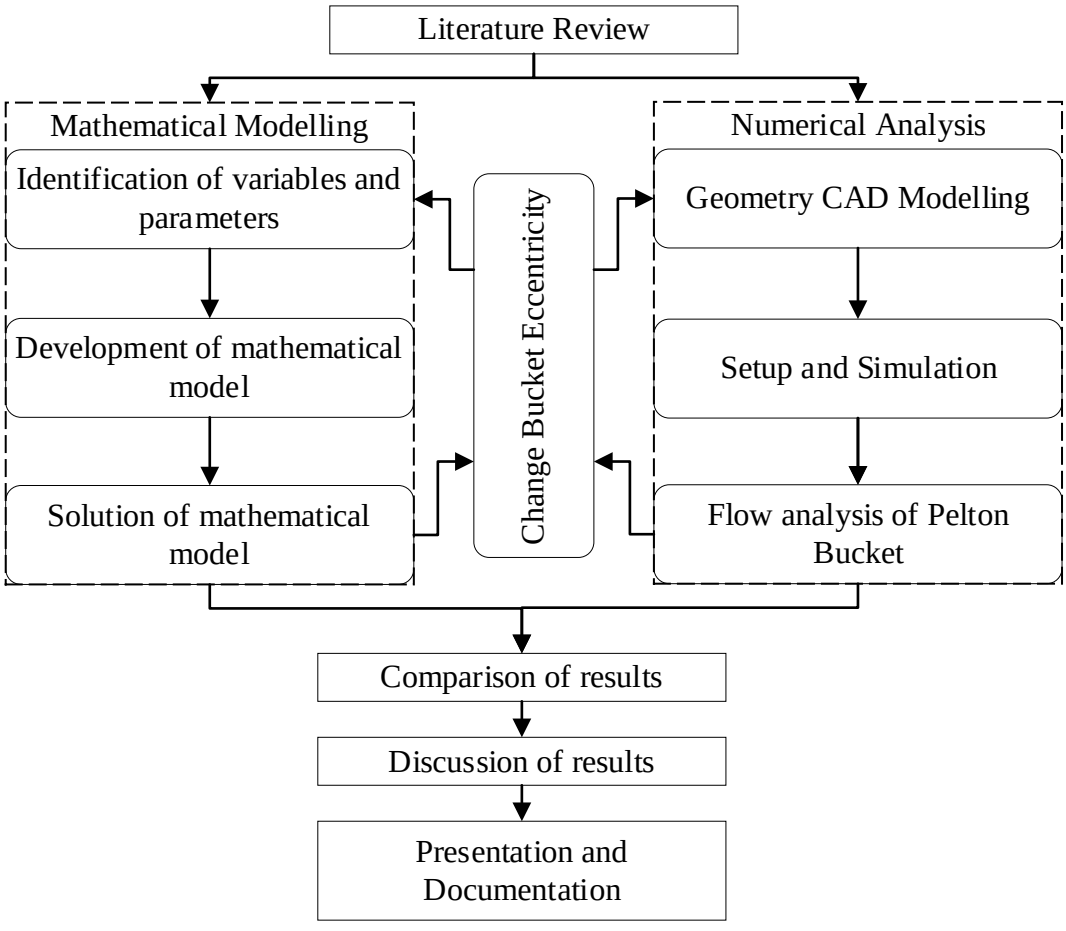

Figure 3.1: Flow diagram of Methodology

3.1 Literature Review

The major portion of the research was covered by the literature review. Books, journals, papers and articles was thoroughly studied and reviewed throughout the project. The literature mainly focusing on the Pelton turbine, bucket, splitter and the alignment of the components was extremely prioritized to obtain the required background for the study. Moreover, in this process the required assumptions and theories was noted so that to be used in the project as explained in Chapter Two.

3.2 Plant Specification

The specifications of the test rig whose bucket is used for the research purpose is shown in Table 3.1. The capacity of plant is 2 kW, 5.345×10^{-3} m^3/s discharge, 0.175 m PCD and 47.719 m net head.

Table 3.1: Plant specifications

Installed Capacity (kW)	2
Speed (rpm)	1500
Pitch Circle Diameter (mm)	175
Net Head (m)	47.719
Discharge (m^3/s)	5.345×10^{-3}

3.3 Mathematical Analysis

The detailed explanation and derivation of the expression of torques for general eccentric conditions is presented in Chapter Four.

3.3.1 Identification of variables and parameters

The variables and parameters required to conduct mathematical analysis are identified. The variables required is taken from the previous published paper and books. Some of the variables are head, discharge, runner speed, force exerted by water jet in whirl and flow directions, torques in X, Y and Z axis and efficiency of turbine.

3.3.2 Development of mathematical model

This step includes study of various relations between parameters and variables involved and development of equations to calculate final torque. The torque equation is developed for an eccentric bucket in general form. Whenever, eccentric angle is 0°, it

denotes normal condition. To deduce the equation, head is considered as given parameter.

3.3.3 Solution of mathematical Model

Calculation is done for velocities and forces taking value of head and eccentric angle as constant. The obtained values were substituted in the torque equation which gave the value of torque for three different conditions about three different global axes.

3.4 Numerical Analysis

The detailed explanation of procedure and setup for the flow analysis for three conditions is presented in Chapter Five.

3.4.1 CAD Model Development

For the numerical analysis of the bucket, CAD model is developed in CATIA V5-6R2017. The dimensions of the model developed is taken from the bucket of the test rig installed in Pulchowk Campus. The developed geometry of bucket is kept eccentric and the analysis is conducted on three conditions, normal condition, 1° and 2° eccentric.

3.4.2 Setup and Simulation

The developed model in CATIA is extracted to ANSYS where the flow analysis is conducted to know the exact flow pattern and losses acquired by the alignment alteration in the model. The necessary boundary conditions and flow parameters is according to the reviewed literature and field conditions. Finally, the simulation is conducted for various iterations unless the flow is fully developed. The obtained results are validated with the results obtained from mathematical calculations conducted in next stage.

3.4.3 Flow analysis

Fluid flow analysis is conducted using CFX code of ANSYS. Simulation is conducted for total time required for wheel to rotate through 140° for three different bucket eccentric conditions. Torque in the middle bucket is monitored which was duplicated later by MATLAB to obtain final total torque.

3.5 Comparison of results

Results obtained from numerical flow analysis is compared with the results from mathematical solution. The results are presented in the form of line chart and compared side by side in Chapter Six.

3.6 Discussion of findings

The error and uncertainties of the obtained results are discussed in further sections. The error obtained are found to be in acceptable range which conforms the accuracy of the model and analysis approach.

3.7 Documentation and presentation of the findings

The findings of the research work are presented in the form of conference article and formal thesis report as per requirement of the guidelines of Department of Mechanical and Aerospace Engineering, Pulchowk Campus, Institute of Engineering.

CHAPTER FOUR: MATHEMATICAL MODEL DEVELOPMENT

4.1 Problem Definition

Whenever the jet interacts with bucket it gets split into two equal halves. The force exerted by two halves in whirl directions are added to get greater effect whereas the force exerted by two halves in flow direction are cancelled out due to opposite to each other in direction. When the bucket gets eccentric, splitter is unable to divide jet into two equal halves and force exerted in flow direction comes into act, which causes angular alignment of jet velocity at inlet with bucket peripheral velocity. This leads to generation of torque in perpendicular to whirl direction. This section basically deals with the calculations involved in torque generated by this eccentric bucket in each direction perpendicular to whirl direction.

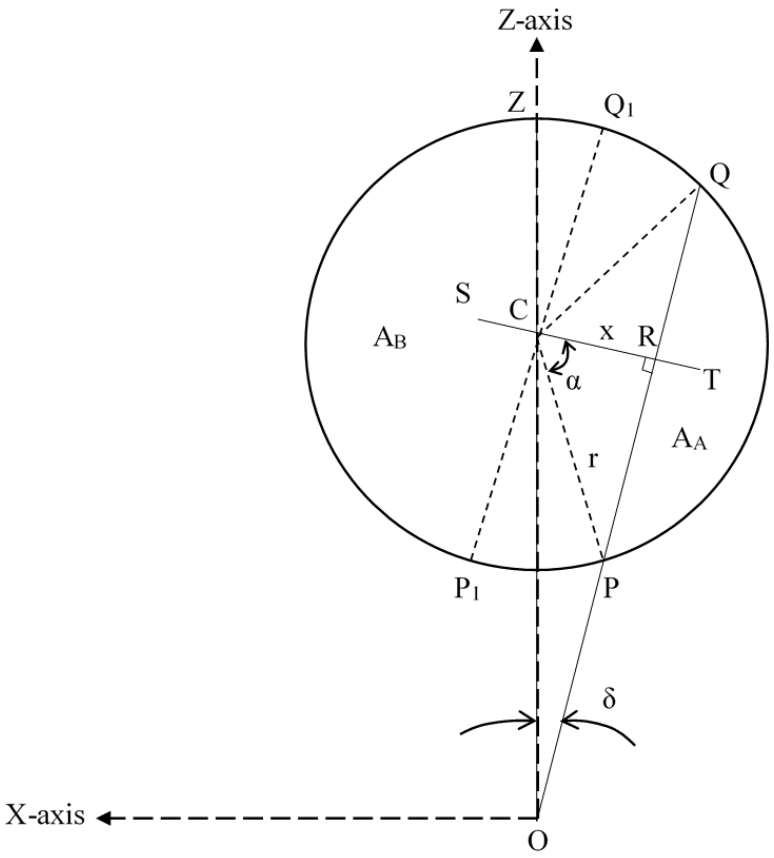

Figure 4.1: Cross section of water jet showing eccentric splitter

4.2 Expression for Normal Force

A circular cross section of water jet with radius ‘r’, center ‘C’ and jet area ‘a’ as shown in Figure *4.1*. OC represents the pitch circle radius and is denoted by ‘R’. The non-

eccentric splitter is represented along Z-axis OZ and when in long run the bucket is displaced by a small angle δ the new position of rotated splitter is represented along PQ. The center of the splitter is displaced by distance x which is represented by CR and the jet is split into two unequal areas, PQRP-the smaller one and PP_1ZQ_1QRP-the larger one. The force is assumed to act on the geometric centroid of split area of jet, T for smaller area and S for larger area. Other parameters and notations are used to obtain the easy calculation of torque generated due to impingement of the jet into the bucket. To commence the calculation values of x and α are needed, which is calculated as,

From triangle OCR,

$$x = R \times sin\delta \qquad \text{Equation 4.1}$$

And, from triangle PCR,

$$x = r \times cos\alpha$$

$$\therefore \alpha = \cos^{-1}\left(\frac{x}{r}\right) \qquad \text{Equation 4.2}$$

The net head available at the turbine inlet is known and inlet velocity and wheel peripheral velocity is calculated as,

$$Inlet\ Velocity(v) = C_v\sqrt{2gH} \qquad \text{Equation 4.3}$$

Similarly,

$$Turbine\ peripheral\ velocity\ (u) = K_u\sqrt{2gH} \qquad \text{Equation 4.4}$$

Where,

$$H = Net\ head\ available\ at\ turbine\ inlet, m$$

$$g = Acceleration\ due\ to\ gravity, m\backslash s^2$$

$$C_v = Coefficient\ of\ velocity$$

$$K_u = Speed\ ratio$$

The force exerted by the jet to the bucket in normal condition and torque generated is calculated by,

$$Force = mass\ flow\ rate \times velocity\ in\ flow\ direction$$

Where,

$$mass\ flow\ rate = density \times jet\ area \times jet\ velocity$$

So, it can be written as,

$$F_y = \rho a v\left(v_{w_{in}} + v_{w_{out}}\right) \qquad \text{Equation 4.5}$$

The force exerted by split jet cannot be approximated by a single portion of jet as done in normal condition. So, two jet areas A_A and A_B determined and force will be calculated separately to obtain final result. Torque generated accordingly will be calculated in each X, Y and Z-axis directions

4.3 Expressions for area A

For Area A:

$$Area\ (A_A) = \frac{r^2}{2}(2\alpha - \sin(2\alpha)) \qquad \text{Equation 4.6}$$

Centroid from splitter PQ is given by:

$$\overline{x}_A = \frac{4rsin^3\alpha}{3(2\alpha - \sin(2\alpha))} - x$$

$$or, \overline{x}_A = \frac{4rsin^3\alpha}{3(2\alpha - \sin(2\alpha))} \times \frac{\frac{r^2}{2}}{\frac{r^2}{2}} - x$$

$$\therefore \overline{x}_A = \frac{2r^3sin^3\alpha}{3 \times \frac{r^2}{2}(2\alpha - \sin(2\alpha))} - x \qquad \text{Equation 4.7}$$

Putting Equation 4.6 in Equation 4.7 we get,

$$\overline{x}_A = \frac{2r^3sin^3\alpha}{3A_A} - x \qquad \text{Equation 4.8}$$

The velocity triangles at inlet and outlet of area A is drawn in Figure *4.2*.

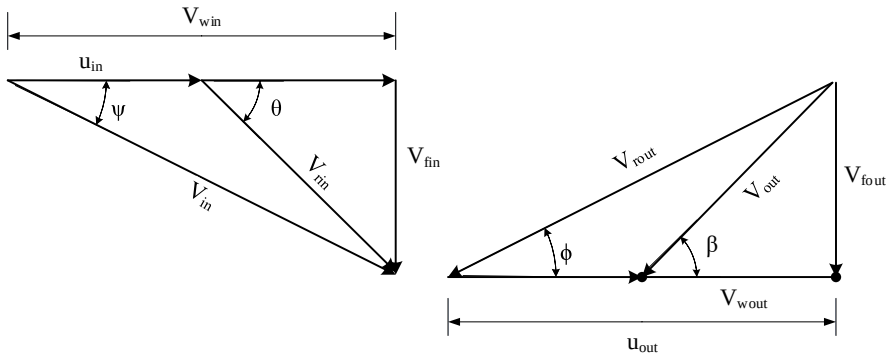

Figure 4.2: Velocity triangle at (a) Inlet and (b) Outlet of Area A

From velocity triangle at Inlet,

$$V_{in} = v$$

$$u_{in} = u$$

$$v_{w\,in} = v cos\psi$$

$$v_{f_{\,in}} = v sin\psi$$

$$v_{r\,in} = \sqrt{\left(V_{w\,in} - u\right)^2 - V_{f\,in}^{\,2}}$$

From velocity triangle at Outlet,

$$u_{out} = u$$

$$v_{r\,out} = v_{r\,in}$$

$$v_{w\,out} = v_{r\,out} cos\phi - u = v_{r\,in} cos\phi - u$$

$$v_{f_{\,out}} = v_{r\,out} sin\phi$$

Then,

$$Mass\ flow\ rate\ (\dot{m}) = \rho A_A v$$

$$Force(F) = Mass\ flow\ rate \times change\ in\ velocity$$

Force exerted in the whirl direction,

$$F_{A_w} = \rho A_A v\left(v_{w_{in}} + v_{w_{out}}\right) \qquad \text{Equation 4.9}$$

Equation 4.9 represents the force exerted in Y-axis direction.

Similarly, force exerted in flow direction is given by,

$$F_{A_f} = \rho A_A v \left(v_{f_{out}} + v_{f_{in}}\right) \qquad \text{Equation 4.10}$$

Equation 4.10 represents the force exerted in X-axis direction.

4.4 Expressions for area B

For Area B:

$$Area\ (A_B) = \frac{r^2}{2}(2\pi - 2\alpha + \sin(2\alpha)) \qquad \text{Equation 4.11}$$

Centroid from splitter is given by:

$$\overline{x}_B = \frac{4rsin^3\alpha}{3(2\pi - 2\alpha + \sin(2\alpha))} + x \qquad \text{Equation 4.12}$$

From Equation 4.11 and Equation 4.12 we can write,

$$\therefore\ \overline{x}_B = \frac{2r^3sin^3\alpha}{3A_B} + x \qquad \text{Equation 4.13}$$

The velocity triangles at inlet and outlet of area B is drawn in Figure *4.3*.

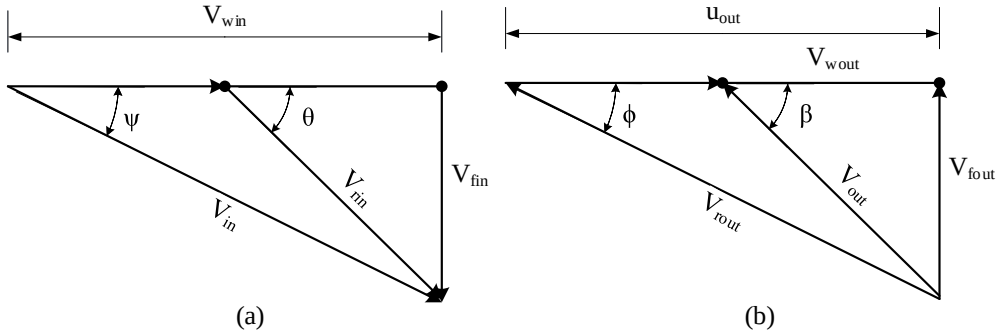

Figure 4.3: Velocity triangle at (a) Inlet and (b) Outlet of Area B

From velocity triangle at inlet,

$$V_{in} = v$$

$$V_{in} = v$$

$$u_{in} = u$$

$$v_{w_{in}} = v cos\psi$$

$$v_{f_{in}} = v sin\psi$$

$$v_{r_{in}} = \sqrt{\left(V_{w_{in}} - u\right)^2 - V_{f_{in}}^2}$$

From velocity triangle at outlet,

$$u_{out} = u$$

$$v_{r_{out}} = v_{r_{in}}$$

$$v_{w_{out}} = v_{r_{out}} cos\phi - u = v_{r_{in}} cos\phi - u$$

$$v_{f_{out}} = v_{r_{out}} sin\phi$$

Then,

$$Mass\ flow\ rate\ (\dot{m}) = \rho A_B v$$

$$Force(F) = Mass\ flow\ rate \times change\ in\ velocity$$

Force exerted by jet in whirl direction is,

$$F_{B_w} = \rho A_B v\left(v_{w_{in}} + v_{w_{out}}\right) \qquad \text{Equation 4.14}$$

Equation 4.14 represents the force exerted in Y-axis direction.

Similarly, force exerted in flow direction is,

$$F_{B_f} = \rho A_B v\left(v_{f_{out}} - v_{f_{in}}\right) \qquad \text{Equation 4.15}$$

Equation 4.15 represents the force exerted in X-axis direction.

4.5 Expression for total torque

The total generated torque is not transmitted to shaft and certain portion of it is lost in the form of various losses. So, $\eta_h, \eta_m\ and\ \eta_v$ be hydraulic, mechanical and volumetric efficiency respectively.

Now, torque generated about X-axis direction is given by,

$$\tau_x = \left(F_{A_w} + F_{B_w}\right) \times R$$

$$\therefore \tau_{x_{shaft}} = \left(F_{A_w} + F_{B_w}\right) \times R \times \eta_h \times \eta_m \times \eta_v \qquad \text{Equation 4.16}$$

Similarly, torque generated about Y-axis is given by,

$$\tau_y = \left(F_{B_f} - F_{A_f}\right) \times R$$

$$\therefore \tau_{y_{shaft}} = \left(F_{B_f} - F_{A_f}\right) \times R \times \eta_h \times \eta_m \times \eta_v \qquad \text{Equation 4.17}$$

Torque about splitter is given by,

$$\tau = F_{B_w} \times \overline{x}_B - F_{A_w} \times \overline{x}_A$$

Now, torque about Z-axis can be obtained as,

$$\tau_Z = \tau \, Cos\delta \qquad \text{Equation 4.18}$$

CHAPTER FIVE: FLOW ANALYSIS IN ANSYS

A general simulation for the analysis of fluid flow in CFX consists of series of processes and works which involves designing of the fluid domain with the help of CAD, discretizing the domain into smaller elements known as meshing, setting up the physics in CFX pre and finally post processing the results to present the outputs in an interactive and very effective way. This general workflow is shown in Figure 5.1.

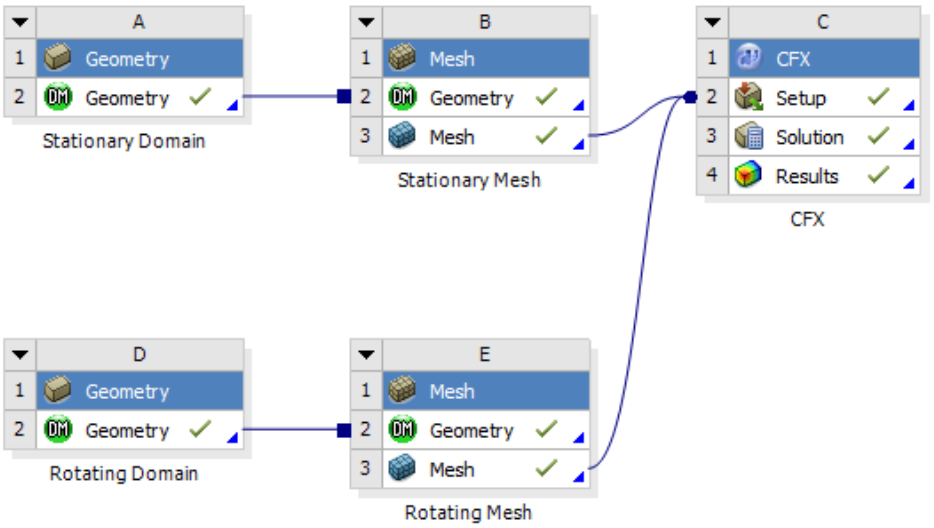

Figure 5.1: Workflow of a simulation in ANSYS Workbench

Computational Fluid Dynamics (CFD) uses highly developed modern computer and ii is applicable in the fields of fluid flow as well as other processes involving various physics (ANSYS, 2011). It takes a pre specified region in which behavior of certains physical phenomena is to be known and solves the equations governing the fluid flow by the use of pre-defined boundary conditions as well as targets to achieve outputs.

The phenomenon of momentum and transfer of heat and mass can be explained by a standard set of general equations expressed in the form of partial differentials known as Navier-Stokes equation. These set of equations do not have any general solution but can be broken into smaller sections and can be applied to specific boundaries to solve the problem computationally with the help of approximating model as in turbulence models. Finite volume method is frequently used technique for solving the fluid flow

problems among various CFD codes. CFX uses this technique which uses the process of dividing the domain into smaller sections known as grids or meshes and then solving.

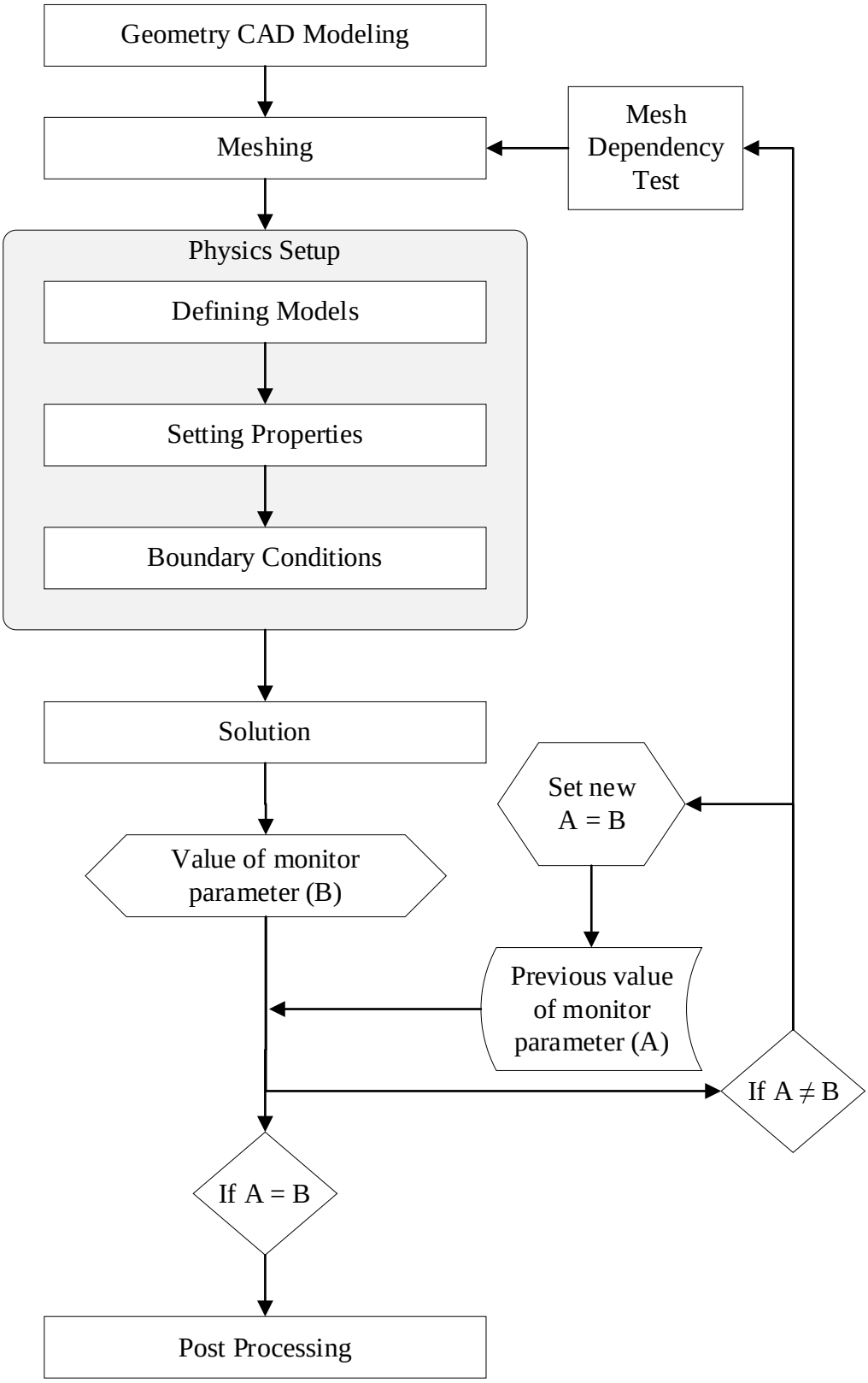

Figure 5.2: Steps in a computational analysis

The equations are converted into discrete form and then solved for each smaller control volume in an iterative way for a specific region. The complete behavior of the fluid flow can be obtained by discretely obtaining the solution of each parameter at specified points all along the region with a precise and systematic approximation. In this section, the complete steps and processes followed to study the fluid flow with the help of computational analysis. The steps also involves the mesh dependency test which assures the selection of optimum number of mesh without compromising the quality of outputs in optimum use of computational cost and time as shown in Figure 5.2.

5.1 CAD modelling of Fluid Domain

The fluid domain was designed using the ANSYS CAD modelling application, DesignModeler. The geometries consisting the fluid domain was quite simple so the DesignModeler was used. The bucket designed in CATIA P3 V5-6 R2017 shown in Figure *5.3* was imported to DesignModeler and Boolean function was used to remove the imported bucket region.

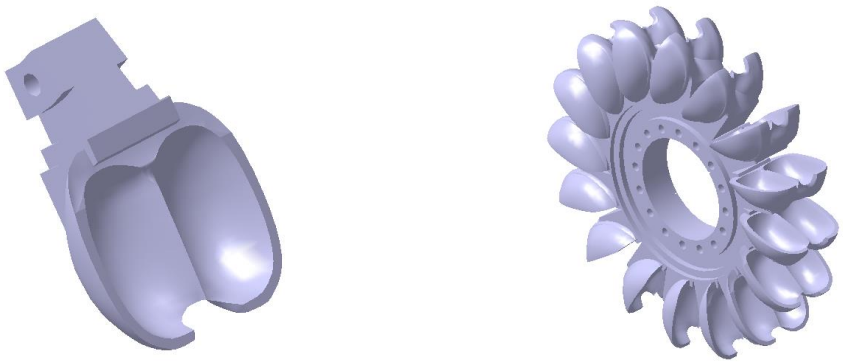

(a) (b)

Figure 5.3: 3D CAD of (a) single bucket and (b) complete runner

Figure *5.4* shows complete CAD drawing of the stationary and rotating domain assembled together which were modeled separately. The stationary domain consists of water jet and a thin layer of air surrounding rotating domain and rotating domain consists of the region around the buckets where water flows excluding the bucket region. The rotating domain rotates and the stationary domain remains fixed during the simulation. Both domains are 140 degrees extended to obtain the complete torque curve. Both domains were connected with an interface between them so that fluid can flow from one domain to another domain without any obstructions.

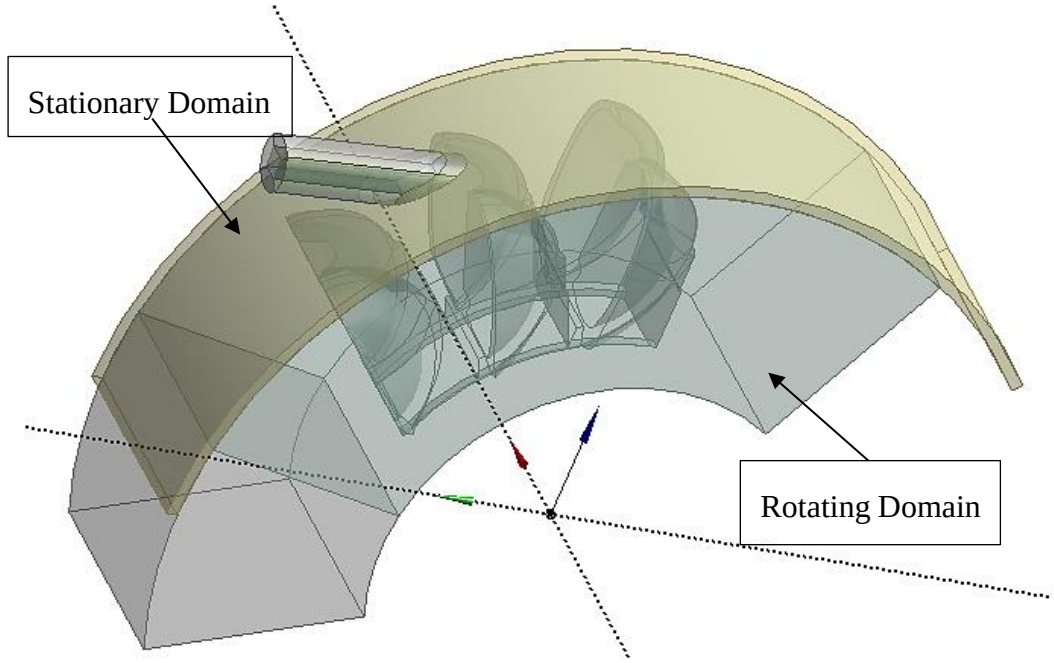

Figure 5.4:Stationary and rotating domain

5.2 Meshing with ANSYS Meshing

It is difficult to find the solution for whole domain in an integral form so an approach of dividing domain into smaller sub regions, known as meshing, is adopted which finds the solution in smaller regions to approximate the outputs of larger domains of interest or study (ANSYS, 2019).

Whenever the meshing is finer, it requires more computational cost and time, to obtain high accurate results with required convergence level. Meshing requires a significant time so highly automated and computerized tool can be used to obtain the results of meshing in an faster and efficient manner also to reduce the overall time required for the simulation process. In this section, detail process followed to obtained the meshing results for both rotating and stationary domains is explained.

Meshing of Rotating Domain

Two standalone meshing components were created for stationary and rotating domain in the ANSYS workbench to mesh both domains separately. The rotating domain consists of complex geometries so it was meshed separately using “advanced size function” turned on. The body sizing with “Body of Influence” was used to cover the water jet region with fine mesh when interacting with all three buckets. Similarly, other two body sizing with “Body of Influence” were used at the water outlet from the bucket

with fine mesh to capture the back flow of water. Since the more focus is given to the middle bucket flow the “Face Sizing” with “Inflation” consisting of smaller elements was used in front face to capture boundary flow at the bucket as shown in Figure 5.5.

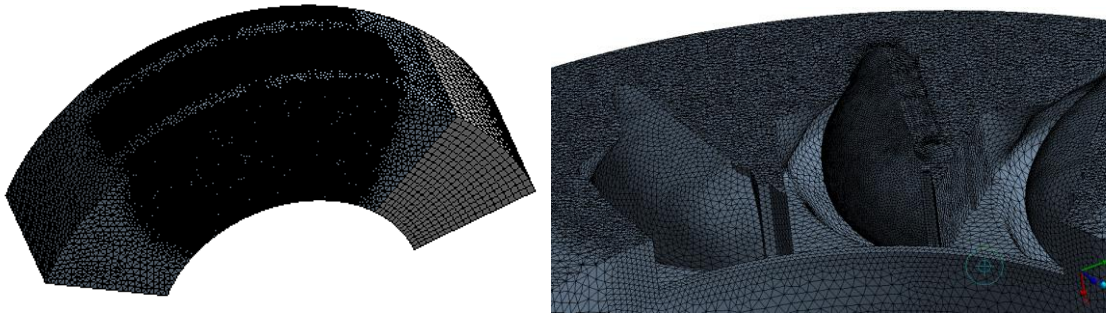

(a) (b)

Figure 5.5: Meshing of (a) Rotating Domain (b) Section showing inner view

Meshing of Stationary Domain

The region for jet was meshed finely and inflation layer was used at the wall of jet which helps to capture the flow at the boundary at the stationary domain. It also helped to study the interaction between water and air at the boundary of the jet. The meshes of stationary domains and jet region is shown in Figure *5.6*.

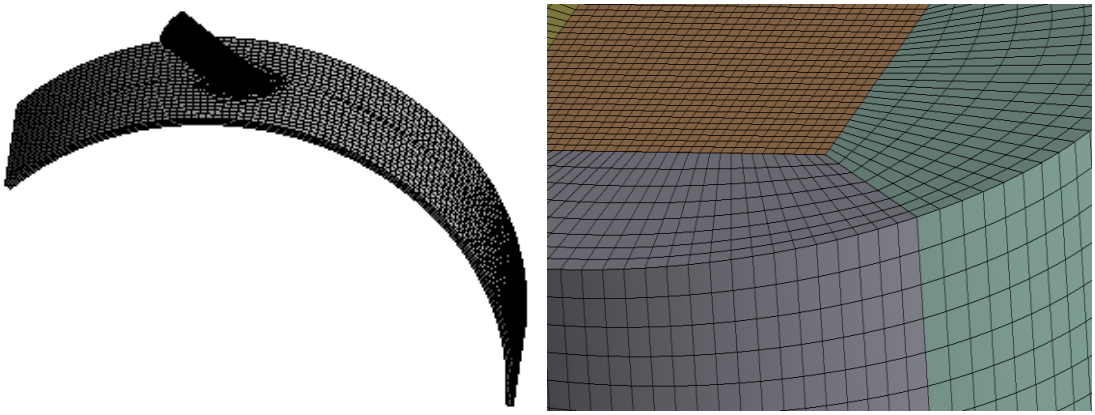

(a) (b)

Figure 5.6: Meshing of (a) Stationary Domain (b) Water jet

5.3 Physics Setup

CFX Pre is inbuilt component used by ANSYS CFX in which all the physics are defined which are used to obtain the solution for a fluid flow problem. For this, two inputs from meshing components are given in a common CFX setup component which combines two meshing components and allows to define all the physics with pre-defined boundary conditions for the purpose of analysis of flow problem.

Analysis Type

To conduct flow analysis in ANSYS CFX Pre, nature of analysis: transient or steady state, total analysis flow time and individual time steps is defined in the "Analysis Type" tab. In this research, the analysis is set to transient with adaptive timesteps as it is dependent in time.

Number of coefficient loops can be selected with adaptive time steps. By doing this, solver can adjust size of the timestep itself. Its maximum and minimum target value can be provided which is used to control the actual number of coefficient loops (ANSYS, 2012). By observing the maximum and minimum value of number of coefficient loops, solver can change the actual number of coefficient loops according to the convergence criteria and time assigned. The full utilization of resources can be achieved by using this approach of adaptive timestep to obtained the desired level of convergence.

The total time of the analysis is set to the time required by a rotating domain to rotate through complete 140 degrees. All the expressions used to define the variables in CFX setup are presented in Table C-1.

Domains

Rotating and stationary domains were separately created in the domain section. The domain type was selected as "Fluid Domain" with coordinate frame selected with origin at center of the wheel. Two fluids, Air and Water were defined with continuous fluid morphology because fluids form continuous connected region throughout the simulation. Since the Pelton buckets are exposed to atmospheric pressure, pressure of 1 atm is used as reference. To capture the effect of gravity Buoyant option was selected for the model of buoyancy in the positive Z-axis direction. The "Buoyancy Reference Density" was set to 1000 kg/m^3, which is approximate density difference between Water and Air.

The flow was multiphase consisting the water and air fluids with homogeneous model. "Homogeneous Model" was chosen because both the phases share the flow field, velocity field, turbulence field and so on near the interface boundary and the droplets are not playing important role in the flow analysis. The "Standard Free Surface Model" was used because the fluid phases are distinct at the interface.

Heat transfer mode was set to none to neglect the heat transfer during the simulation. Heat is generated due to friction between buckets and water flow in the expense of kinetic energy of water which is neglected considering very small temperature difference.

“Surface Tension Coefficient” was set to 0.7 N/m in the “Fluid Pair Models” tab to capture the nature of interaction between water and air in this multiphase condition. The primary fluid was set to water with continuum surface force surface tension model.

The initialization tab sets the initial conditions for each domain overriding the global initial conditions. Since the analysis is transient in nature the initial conditions are set. Each cartesian velocity component is set to zero with relative static pressure of 0 Pa. Initial volume fraction for air and water was set to 1 and 0 respectively assuming that the domains are fully covered by air at the initial phase.

To provide the rotation to rotating domain, “Domain Motion” was set to Rotating with the Angular Velocity equal to expression “AngVel”. The rotation was provided along positive X-axis. For the stationary domain, Domain Motion was set to stationary.

Boundary Conditons

While defining the boundary conditions a naming with abbreviations was followed to maintain the short boundary names. Each three buckets is named as Bottom (B), Middle (M) and Top (T) with two boundary names. Middle bucket consists of two boundaries namely, MB for the main flow region and MBC for the complete middle bucket surface. Similarly, TB, TBC for top bucket and BB, BBC for bottom bucket were defined. The buckets were defined as smooth wall with no slip conditions.

When water enters the rotating domain, the air is pushed out of the rotating domain through the openings named as “RotOpen” set to as “Opening” to entertain the flow of air in and out. The initial volume fraction of air at “RotOpen” was set to 1 with relative pressure of 0 Pa. Similar values were defined for the “StatOpen” which corresponds the opening boundary at stationary domain.

The “JetWall” boundary was defined as a wall with no slip conditions and smooth wall. This appears as a wall covering the jet and air surrounding the jet. The interaction between the water and air can be studied This helps to study the interaction of water with air at the water jet boundary region.

Inlet was defined at the JetInlet surface with the normal inlet velocity set to the InletVel expression as defined in the setup. In the initial condition the theoretical inlet velocity and angular velocity was used to simplify the nature of simulation. For the air the volume fraction was set to 0 and it was set to 1 for the water in that surface.

"StatInlet" was defined as the inlet for the air flow with very small initial velocity and at this surface the volume fraction of air was set to 1 and for water it is set to 0.The volume fraction of air and water was set to 1 and 0 respectively. This air inlet was defined to simulate the real scenario of air entering the Pelton rig while operation from the near surrounding.

Solver Control and Output Control

The main required output is the total torque on the middle bucket which was monitored throughout the simulation. The expressions "TorqueMBC", "TorqueMBCy" and TorqueMBCz" were set in the monitor section to capture the torque in middle bucket in each three axes x, y and z respectively saving output results in each timestep which makes the torque curves smoother.

5.4 Solution using CFX-Solver Manager

CFX-Solver Manager was used to conduct the simulation to obtain the solution with convergence criteria of previously set target. An overview of other physics as well as hardware setup which is used to conduct the flow analysis is presented in Table 5.1.

Table 5.1: Basic setup and hardware specifications

Solver	ANSYS CFX 19.0
Time Discretization	Transient
Advection Scheme	High Resolution
Transient Scheme	Second Order Backward Euler
Turbulence Model	SST with automatic wall function
Multiphase Model	Homogeneous model with standard Free Surface Model
Surface Tension Model	Continuum Surface Force with primary fluid as water
Convergence Criteria	RMS with Residual Target of 1.15×10^{-4}
Hardware	Processor: Intel® Core™ i5-8400 @ 2.80 GHz 2.81 GHz Number of Cores: 6 Memory: 16 GB

5.5 Post Processing

The torque form simulation was obtained at the middle bucket only so the post processing was required to duplicate the obtained torque and obtain total torque. The changing timestep size due to adaptive timesteps made the problem quite complicated so MATLAB coding was preferred instead of Excel table operation. The code used for duplicating torque curve is presented in APPENDIX D: The bucket frequency is calculated as $f_Z = \frac{\omega Z}{2\pi}$ which gave the time period of single bucket as $t = \frac{1}{f_z}$. To find the total torque, torque obtained from single bucket was shifted and it was duplicated 'n' times and each torque curves were shifted by $n \times \frac{1}{f_Z}$ seconds. This gives a steady state reading of the torque in a certain portion.

5.6 Mesh dependency test

The solution of numerical models is highly dependent to the solver grid. If computational resources are available are easily accessible, it is always recommended to adapt the grid until the solution does not depend on the mesh. When grid independence is obtained, a larger and independent mesh should be used for the further analysis to save computational resources (Petley, 2018). The details of number of elements and all sizing used for all mesh set for the purpose of mesh dependency test is presented in Table 5.2.

Table 5.2: Overview of the mesh dependency tests showing number of elements and elements sizing

Mesh Set	No. of Elements			Element Sizing (mm)		
	Stationary	Rotating	Total	Face Sizing	Body of Influence	First Layer Height
M1	1,681	250,544	252,225	1.00	3.00	-
M2	24,780	450,726	475,506	0.90	2.00	1
M3	55,584	2,058,139	2,113,723	0.80	1.00	0.5
M4	137,341	2,989,709	3,127,050	0.50	0.90	0.3
M5	152,609	4,750,979	4,903,588	0.35	0.80	0.2

A vertex centered scheme is used by the CFX in which all the parameters are kept at the vertex of the cell where the solver-element or control volume is taken as the dual for the element of the mesh (ANSYS, 2013). Skewness is irrelevant to be used as a quality measurement parameter as CFX uses vertex as the center of the solver-element. The parameters used by the CFX as a quality measurement parameters are listed in

Table 5.3 which is updated frequently whenever the deformation of mesh occurs (ANSYS, 2011).

Table 5.3: Criteria for mesh quality in CFX.

Type	Good	Acceptable	Poor
Minimum Orthogonal Angle	> 50	50 > M > 20	< 20
Maximum Expansion factor	< 5	5 < M < 20	> 20
Maximum Aspect Ratio	< 100	100 < M < 1000	> 1000

Table 5.4 shows the quantity of nodes expressed in percentage, which satisfy the good quality criteria as presented in Table 5.3. The quantity of nodes conforming the good quality criteria are all above 92%, which shows the approach of meshing is acceptable for the analysis.

Table 5.4: The quantity of nodes (%) conforming the good quality criteria

Mesh Set	Min. Orthogonal Angle		Max. Expansion Factor		Max. Aspect Ratio	
	Stationary	Rotating	Stationary	Rotating	Stationary	Rotating
M1	92	100	100	98	100	100
M2	92	99	94	97	100	100
M3	92	100	97	99	100	100
M4	96	100	99	98	100	100
M5	96	100	98	96	100	100

Table 5.5 shows the comparison of torque generated in the shaft about wheel-rotating axis obtained from the mathematical calculation and simulation. Percentage error is calculated to select the best model with less error. More mesh sets were not created when the error was changed by less than 0.2%. Finally, mesh set M3 is selected for the further analyses.

Table 5.5: Comparison of averaged value of torque from simulation with calculated value and its error

Mesh Set	Mean Torque (Nm)		Error (%)	Remarks
	Simulation	Calculated		
M1	11.809	12.673	6.812	-
M2	12.355	12.673	2.502	-
M3	12.570	12.673	0.811	Selected
M4	12.593	12.673	0.625	-
M5	12.601	12.673	0.562	-

Figure 5.7 shows that when number of mesh elements were further increased after mesh set M3, the error remained almost constant. So, mesh set M3 was selected to reduce the computational cost and time considering the resources available.

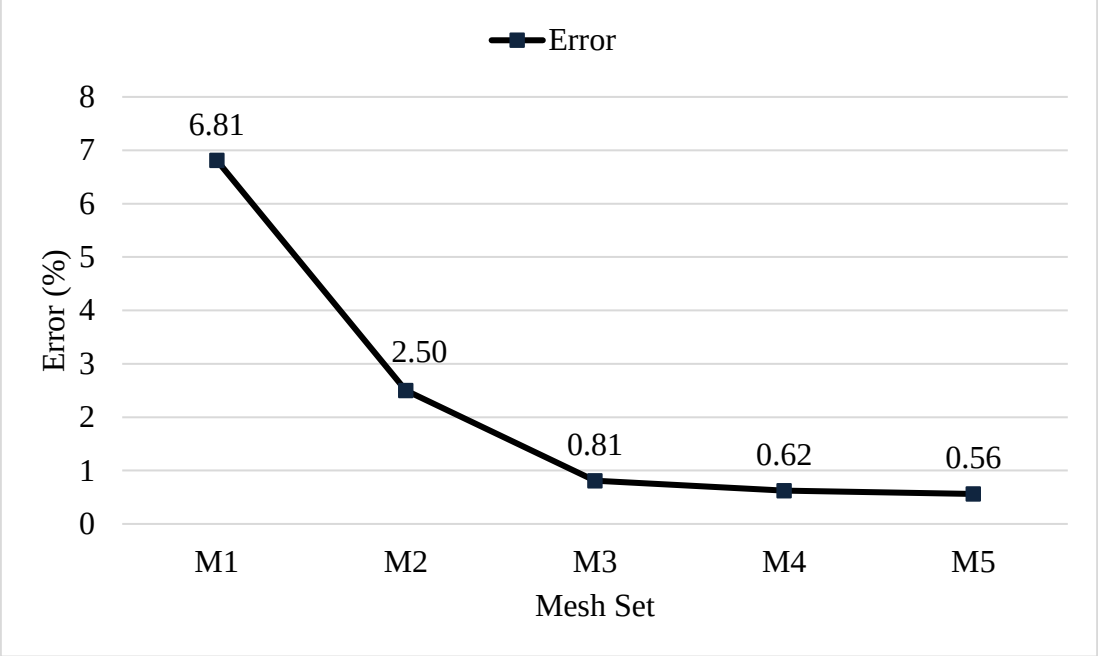

Figure 5.7: Error (%) of torque in all Mesh set used for mesh dependency test

CHAPTER SIX: RESULTS AND DISCUSSION

6.1 Results from mathematical calculation

6.1.1 Torque calculation for normal condition

The pitch circle radius (R) is taken as 0.0875 m as known quantity. The eccentric length x is given by Equation 4.1,

$$x = R \times sin\delta$$

For, normal condition, $\delta = 0°$, so,

$$x = 0.0875 \times sin0° = 0$$

Now, given jet radius as $r = 0.0075$ m and using Equation 4.2,

$$\therefore \alpha = \cos^{-1}\left(\frac{x}{r}\right) = \cos^{-1}\left(\frac{0}{0.0075}\right) = 90°$$

We have , $Net\ head\ (H) = 47.719\ m$, $g = 9.81\ m/s^2$, $C_v = 0.98$ and $K_u = 0.45$. Using Equation 4.3 and Equation 4.4, we get, $v = 29.986\ m/s$ and $u = 13.769\ m/s$.

At inlet,

$$V_{in} = 29.986\ m/s$$

$$u_{in} = 13.769\ m/s$$

Here, $\psi = \delta = 0°$

$$v_{w_{in}} = vcos\psi = 29.986\ m/s$$

$$v_{f_{in}} = vsin\psi = 0\ m/s$$

$$v_{r_{in}} = v - u = 16.217\ m/s$$

At outlet,

$$u_{out} = 13.769\ m/s$$

$$v_{r_{out}} = v_{r_{in}} = 16.217\ m/s$$

Here, $\phi = 15°$

$$v_{w_{out}} = v_{r_{out}}cos\phi - u = 1.895\ m/s$$

$$v_{f_{out}} = v_{r_{out}} sin\phi = 4.197\ m/s$$

Also,

$$\rho = 1000\ kg/m^3\ for\ water$$

$$a = \pi r^2 = 0.000176715\ m^2$$

Then, force exerted in whirl direction is given by,

$$F_w = \rho a v\left(v_{w_{in}} + v_{w_{out}}\right) = 168.939\ N$$

Taking $\eta_h = 0.95, \eta_m = 0.94,\ and\ \eta_v = 0.96$ so, torque about X-axis is,

$$\tau_{x_{shaft}} = 14.782 \times 0.95 \times 0.96 \times 0.94 = 12.673\ Nm$$

In normal condition the force exerted in the flow direction cancel each other being equal and opposite. So,

$$\tau_{y_{shaft}} = \tau_z = 0\ Nm$$

6.1.2 Torque Calculation for 1° eccentric bucket

For Area A:

Here, $\delta = 1°$, so,

$$\mathrm{x} = \mathrm{R} \times sin\delta$$

$$\therefore x = 0.0875 \times sin1° = 0.001527\ m$$

Now, given jet radius as $r = 0.0075$ m and using Equation 4.2,

$$\therefore \alpha = \cos^{-1}\left(\frac{x}{r}\right) = \cos^{-1}\left(\frac{00.001527}{0.0075}\right) = 78.252°$$

The area is given by,

$$Area\ (A_A) = \frac{r^2}{2}(2\alpha - \sin(2\alpha)) = 6.561 \times 10^{-5}\ m^2$$

Centroid from splitter PQ is given by:

$$\overline{x}_A = \frac{2r^3 sin^3\alpha}{3A_A} - x = 0.002496\ m$$

Inlet velocity (v) and wheel peripheral velocity (u) is same as the normal condition calculated in section 6.1.1.

At inlet,

$$V_{in} = 29.986\ m/s$$

$$u_{in} = 13.769\ m/s$$

Here, $\psi = \delta = 1°$

$$v_{w_{in}} = v cos\psi = 29.981\ m/s$$

$$v_{f_{in}} = v sin\psi = 0.5233\ m/s$$

$$v_{r_{in}} = \sqrt{\left(V_{w_{in}} - u\right)^2 - V_{f_{in}}^2} = 16.221 m/s$$

At outlet,

$$u_{out} = 13.769\ m/s$$

$$v_{r_{out}} = v_{r_{in}} = 16.221\ m/s$$

Here, $\phi = 15°$

$$v_{w_{out}} = v_{r_{out}} cos\phi - u = 1.899\ m/s$$

$$v_{f_{out}} = v_{r_{out}} sin\phi = 4.198\ m/s$$

Then, force exerted in the whirl direction,

$$F_{A_w} = \rho A_A v\left(v_{w_{in}} + v_{w_{out}}\right) = 62.722\ N$$

Similarly, force exerted in flow direction is given by,

$$F_{A_f} = \rho A_A v\left(v_{f_{out}} + v_{f_{in}}\right) = 9.289\ N$$

For Area B:

$$Area\ (A_B) = \frac{r^2}{2}(2\pi - 2\alpha + \sin(2\alpha)) = 0.0001111\ m^2$$

Centroid from splitter is given by:

$$\overline{x}_B = \frac{2r^3 sin^3\alpha}{3A_B} + x = 0.0039\ m$$

From velocity triangle at inlet,

$$V_{in} = 29.986\ m/s$$

$$u_{in} = 13.769\ m/s$$

Here, $\psi = \delta = 1°$

$$v_{w_{in}} = v cos\psi = 29.981\ m/s$$

$$v_{f_{in}} = v sin\psi = 0.5233\ m/s$$

$$v_{r_{in}} = \sqrt{\left(V_{w_{in}} - u\right)^2 - V_{f_{in}}^2} = 16.221 m/s$$

Similarly, at outlet,

$$u_{out} = 13.769\ m/s$$

$$v_{r_{out}} = v_{r_{in}} = 16.221\ m/s$$

Here, $\phi = 15°$

$$v_{w_{out}} = v_{r_{out}} cos\phi - u = 1.899\ m/s$$

$$v_{f_{out}} = v_{r_{out}} sin\phi = 4.198\ m/s$$

Then, force exerted by jet in whirl direction is,

$$F_{B_w} = \rho A_B v\left(v_{w_{in}} + v_{w_{out}}\right) = 106.213\ N$$

Similarly, force exerted in flow direction is,

$$F_{B_f} = \rho A_B v\left(v_{f_{out}} - v_{f_{in}}\right) = 12.243\ N$$

Now, torque generated about X-axis direction is given by,

$$\tau_{x_{shaft}} = 12.6721\ Nm$$

Similarly, torque generated about Y-axis is given by,

$$\therefore \tau_{y_{shaft}} = -0.207\ Nm$$

$$-ve\ sign\ indicates\ torque\ is\ directed\ towards\ negative\ Y - axis$$

Torque about splitter is given by,

$$\tau = F_{B_w} \times \overline{x}_B - F_{A_w} \times \overline{x}_A = 0.25797\ Nm$$

Now, torque about Z-axis can be obtained as,

$$\tau_Z = \tau\ Cos\delta = 0.25793\ Nm$$

6.1.3 Torque Calculation for 2° eccentric bucket

For Area A:

Here, $\delta = 2°$, so,

$$x = R \times sin\delta$$

$$\therefore x = 0.0875 \times sin2° = 0.003053\ m$$

Now, given jet radius as $r = 0.0075$ m and using Equation 4.2,

$$\therefore \alpha = \cos^{-1}\left(\frac{x}{r}\right) = \cos^{-1}\left(\frac{0.003053}{0.0075}\right) = 65.973°$$

The area is given by,

$$Area\ (A_A) = \frac{r^2}{2}(2\alpha - \sin(2\alpha)) = 4.385 \times 10^{-5}\ m^2$$

Centroid from splitter PQ is given by:

$$\overline{x}_A = \frac{2r^3 sin^3\alpha}{3A_A} - x = 0.001833\ m$$

Inlet velocity (v) and wheel peripheral velocity (u) is same as the normal condition calculated in section 6.1.1.

At inlet,

$$V_{in} = 29.986\ m/s$$

$$u_{in} = 13.769\ m/s$$

Here, $\psi = \delta = 2°$

$$v_{w_{in}} = vcos\psi = 29.967\ m/s$$

$$v_{f_{in}} = vsin\psi = 1.0465\ m/s$$

$$v_{r_{in}} = \sqrt{\left(V_{w_{in}} - u\right)^2 - V_{f_{in}}^{\ 2}} = 16.232\ m/s$$

At outlet,

$$u_{out} = 13.769\ m/s$$

$$v_{r_{out}} = v_{r_{in}} = 16.232\ m/s$$

Here, $\phi = 15°$

$$v_{w_{out}} = v_{r_{out}} cos\phi - u = 1.910\ m/s$$

$$v_{f_{out}} = v_{r_{out}} sin\phi = 4.201\ m/s$$

Then, force exerted in the whirl direction,

$$F_{A_w} = \rho A_A v\left(v_{w_{in}} + v_{w_{out}}\right) = 41.917N$$

Similarly, force exerted in flow direction is given by,

$$F_{A_f} = \rho A_A v\left(v_{f_{out}} + v_{f_{in}}\right) = 6.9\ N$$

For Area B:

$$Area\ (A_B) = \frac{r^2}{2}(2\pi - 2\alpha + \sin(2\alpha)) = 0.000132\ m^2$$

Centroid from splitter is given by:

$$\overline{x}_B = \frac{2r^3 sin^3\alpha}{3A_B} + x = 0.00467\ m$$

From velocity triangle at inlet,

At inlet,

$$V_{in} = 29.986\ m/s$$

$$u_{in} = 13.769\ m/s$$

Here, $\psi = \delta = 2°$

$$v_{w_{in}} = vcos\psi = 29.967\ m/s$$

$$v_{f_{in}} = vsin\psi = 1.0465\ m/s$$

$$v_{r_{in}} = \sqrt{\left(V_{w_{in}} - u\right)^2 - V_{f_{in}}^2} = 16.232\ m/s$$

At outlet,

$$u_{out} = 13.769\ m/s$$

$$v_{r_{out}} = v_{r_{in}} = 16.232\ m/s$$

Here, $\phi = 15°$

$$v_{w_{out}} = v_{r_{out}} cos\phi - u = 1.910\ m/s$$

$$v_{f_{out}} = v_{r_{out}} sin\phi = 4.201\ m/s$$

Then, force exerted by jet in whirl direction is,

$$F_{B_w} = \rho A_B v\left(v_{w_{in}} + v_{w_{out}}\right) = 127.005\ N$$

Similarly, force exerted in flow direction is,

$$F_{B_f} = \rho A_B v\left(v_{f_{out}} - v_{f_{in}}\right) = 12.569\ N$$

Now, torque generated about X-axis direction is given by,

$$\tau_{x_{shaft}} = 12.6711\ Nm$$

Similarly, torque generated about Y-axis is given by,

$$\therefore \tau_{y_{shaft}} = -0.3967\ Nm$$

$$-ve\ sign\ indicates\ torque\ is\ directed\ towards\ negative\ Y - axis$$

Torque about splitter is given by,

$$\tau = F_{B_w} \times \overline{x}_B - F_{A_w} \times \overline{x}_A = 0.5158\ Nm$$

Now, torque about Z-axis can be obtained as,

$$\tau_Z = \tau\ Cos\delta = 0.5155\ Nm$$

Summary of the torque for each condition about all three axes is presented in Table 6.1.

Table 6.1: Torque about X, Y and Z-axis with varied eccentric angle

Eccentricity (δ)	Torque (Nm)		
	X-axis	Y-axis	Z-axis
0°	12.673	0	0
1°	12.672	-0.206	0.257
2°	12.671	-0.396	0.515

6.2 Results from flow analysis

Nowadays, CFD is highly preferred and there are several packages which assist the user with highly interactive and visually attractive graphical presentation features to study the outputs. These graphically interactive results involve the 3D geometry, meshing results, plots and contour and changing the nature of view which involves translating, rotating and scaling (Malalasekera & Versteeg, 2007).

Modern computers are equipped with highly powerful components so they assist the CFD packages to display its results in the form of highly interactive animations and also provide facilities to export those results to other formats so that they can be used for further post processing or presenting the results as per the requirements of the user. In this section, the results, which are obtained from the CFX-Post and then post processed are presented in a graphical form consisting of tables, figures, plots, contours and charts.

Figure 6.1 shows the flow comparison on non-eccentric, 1° eccentric and 2° eccentric bucket at five different angular positions, displaying water volume fraction above 0.7. The volume fraction above 0.7 is only displayed in the figure because showing lower volume fraction makes the water flow appear cloudy making visibility slightly difficult. The colour represents the velocity of water at that frame. One side of bucket is bearing more load of water causing the generation of unbalanced torques. Angular position 88° to 100° shows middle bucket bearing more back-splash in eccentric bucket on one side. It can be seen that, the incoming bucket bears more water pressure in its front at one side due to uneven split of water jet and at one side of back due to uneven backsplash of water from the outgoing bucket for an eccentric condition.

Angular position	Non eccentric	1° eccentric	2° eccentric
64°	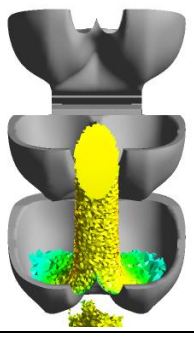	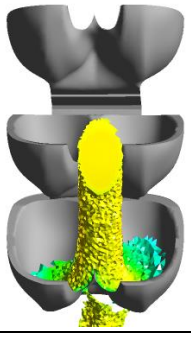	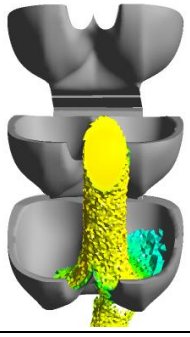
76°	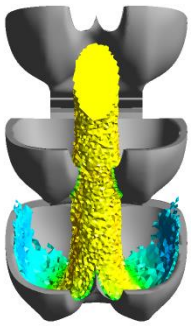	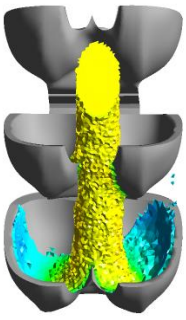	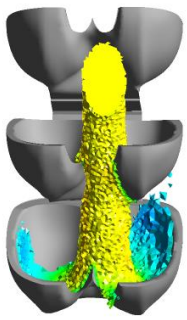
88°	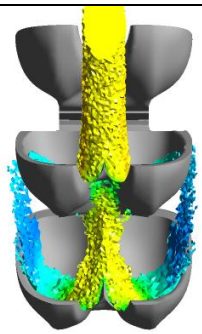	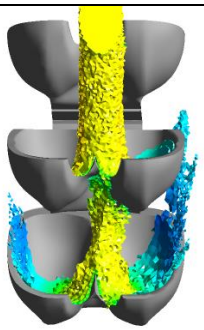	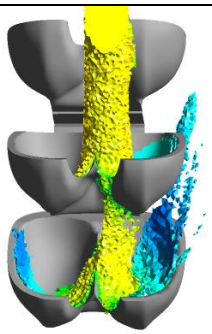
100°	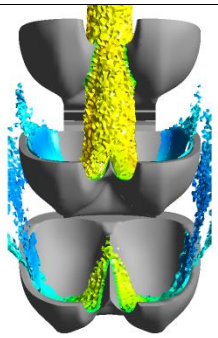	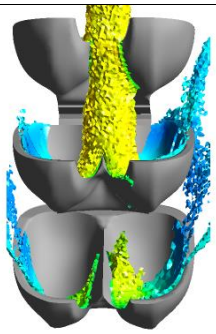	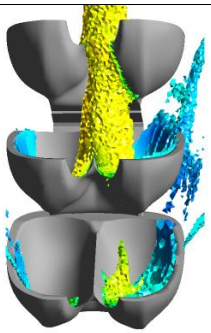
112° 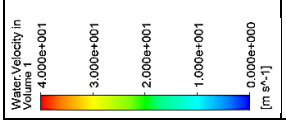	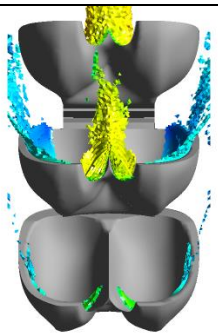	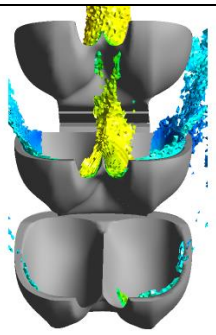	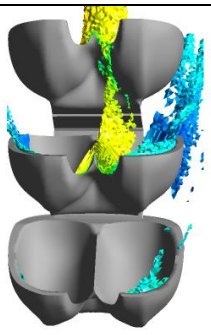

Figure 6.1: Flow comparison in non-eccentric and eccentric bucket

Figure 6.2 shows the contour of water volume fraction for non-eccentric, 1° eccentric and 2° eccentric bucket at same timestep at mid plane perpendicular to turbine axis. The water leaking from the middle bucket is more in the eccentric conditions compared to the non-eccentric condition shown by the black circle. The volume fraction 1 represents cell fully covered by water and 0 represents cell fully covered by air. The incoming bucket influences more on water jet on eccentric condition and at the initial interaction of bucket and jet the splashing of water is more for eccentric bucket which is depicted in the figure.

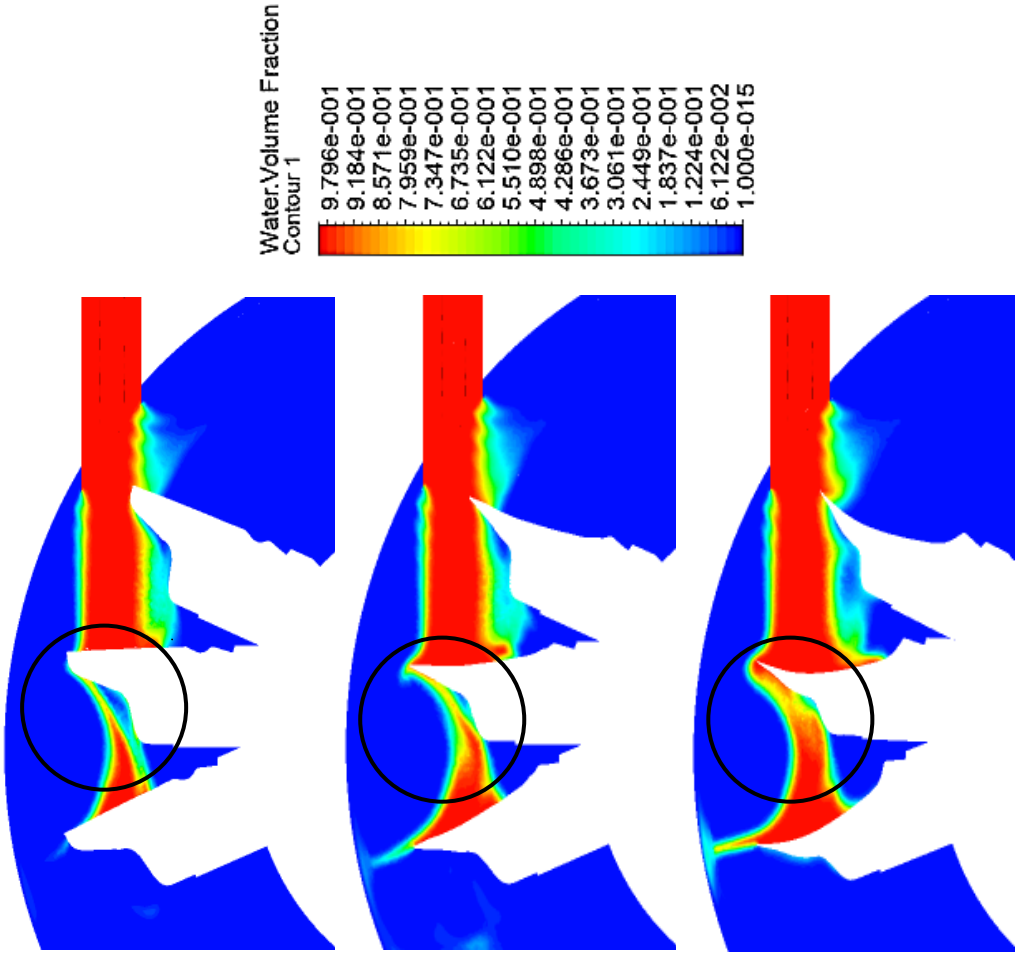

(a) (b) (c)

Figure 6.2: Water volume fraction at mid plane perpendicular to turbine axis at (a) non eccentric (b) 1° eccentric (c) 2° eccentric bucket

Figure 6.3 shows the contour of water volume fraction for non-eccentric, 1° eccentric and 2° eccentric bucket at same timestep at jet mid plane parallel to jet. Water striking the bucket is more on side of bucket for eccentric conditions. This causes more water volume striking and increased pressure in one side of the bucket. Small fraction of water gets deviated and splashes out of jet trajectory due to direct impingement of jet into the

one side of bucket. This supports hydraulic loss which in turn decreases the overall efficiency of wheel.

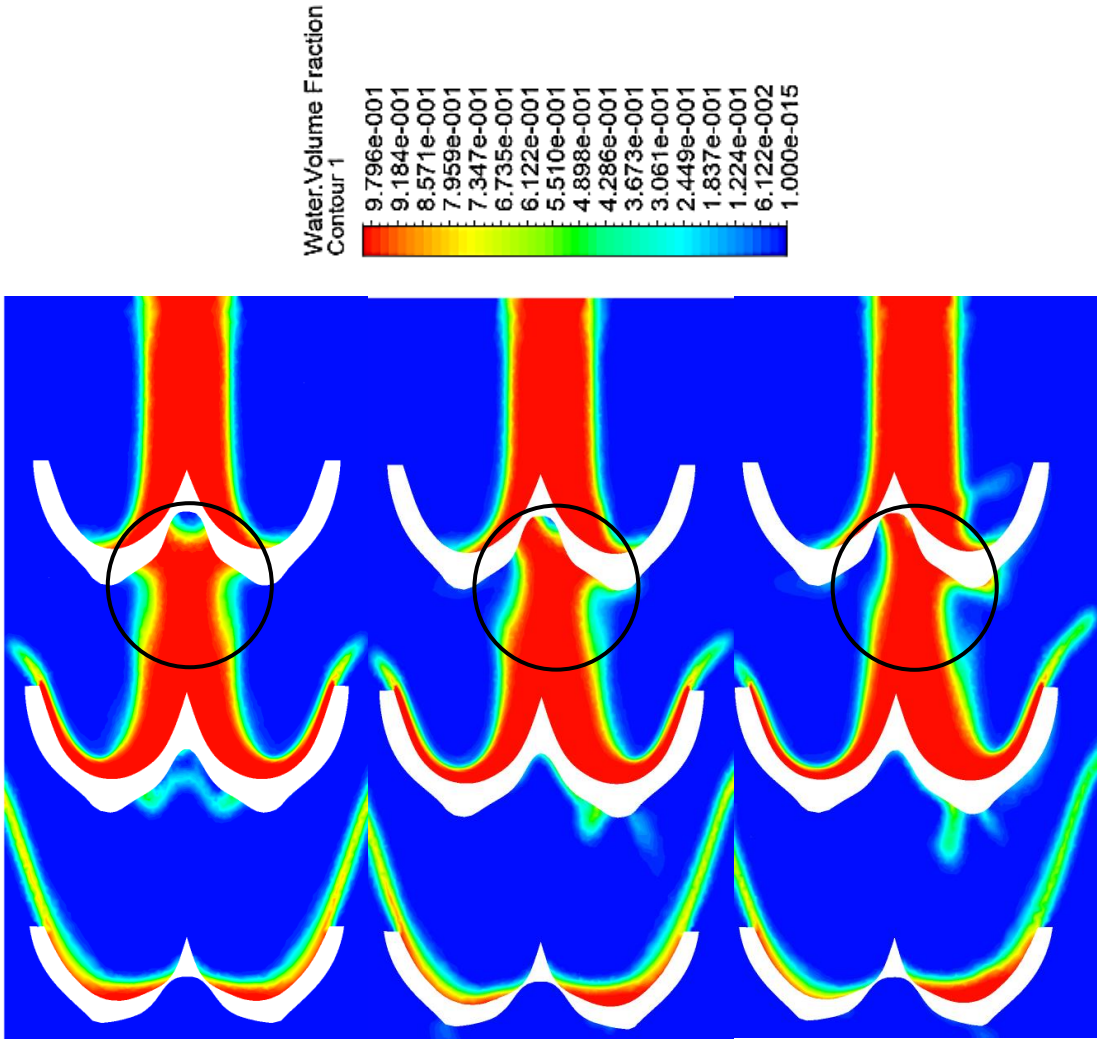

(a) (b) (c)

Figure 6.3: Water volume fraction at jet mid plane parallel to jet at (a) non eccentric (b) 1° eccentric (c) 2° eccentric bucket

Figure 6.4 shows the pressure values in the inner surface of the bucket at the pitch circle diameter. The zero value corresponds to the position of splitter for non-eccentric bucket. The eccentric direction is towards negative axial direction which makes more water to hit the bucket side which is towards the positive axial direction from splitter. Whereas, in the other half of bucket, less pressure is experienced due to smaller volume of water jet striking the side. This imposes more pressure in the bucket in one side and the graph represents the same. The pressure for the eccentric bucket is increasing in positive axial direction side with the increase in eccentric angle. The maximum pressure

for the non-eccentric, 1° eccentric and 2° eccentric bucket is found to be 107.682 kPa, 125.765 kPa and 137.248 kPa respectively.

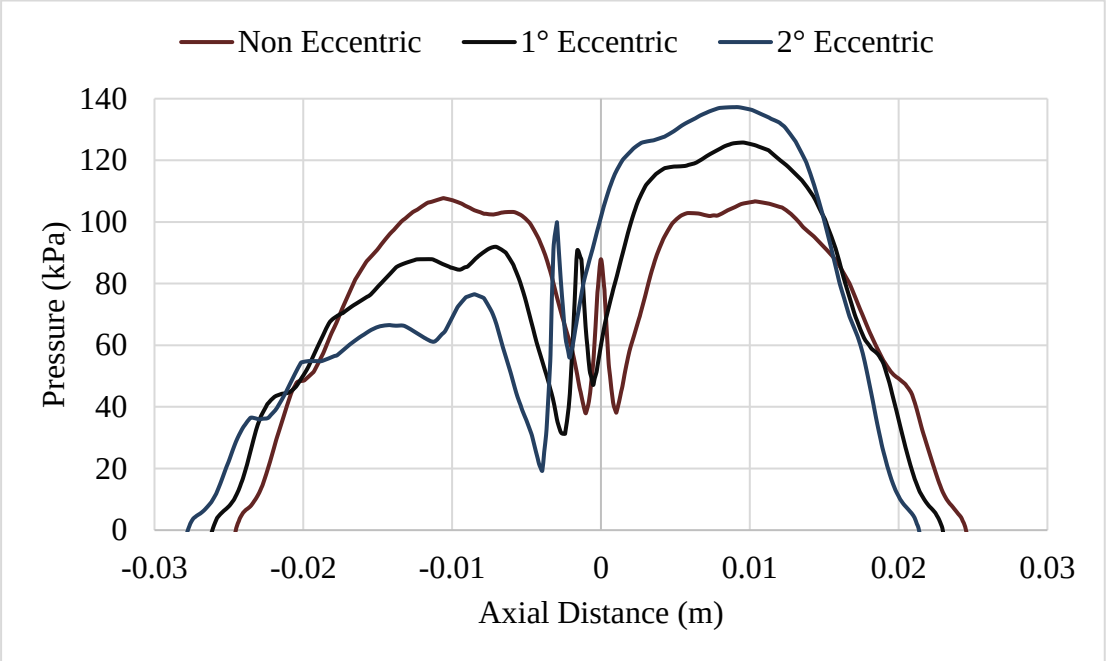

Figure 6.4: Pressure at bucket mid plane along axial distance

Figure 6.5 shows the velocity of water in the inner surface of the bucket at the pitch circle diameter. The orientation of bucket and eccentricity is same as explained in Figure 6.4. More water strikes the bucket side in the positive axial direction which causes disturbance in flow due to direct impingement of water to the bucket ceasing the proper sliding of water through the bucket. This reduces the velocity of water at that portion. Whereas in the other half of bucket smaller volume of water jet striking is occurred which completes its way out to the bucket starting with a proper slide from the bucket splitter and experiencing lesser volume of water having direct impingement. This helps to maintain the velocity of water with a minimum loss. This causes a velocity difference in two sides of the bucket and the graph represents the same. The velocity for the eccentric bucket is decreasing in negative axial direction with the increase in eccentric angle. The maximum velocity for non-eccentric, 1° eccentric and 2° eccentric bucket is found to be 27.724 m/s, 28.688 m/s and 29.444 m/s respectively.

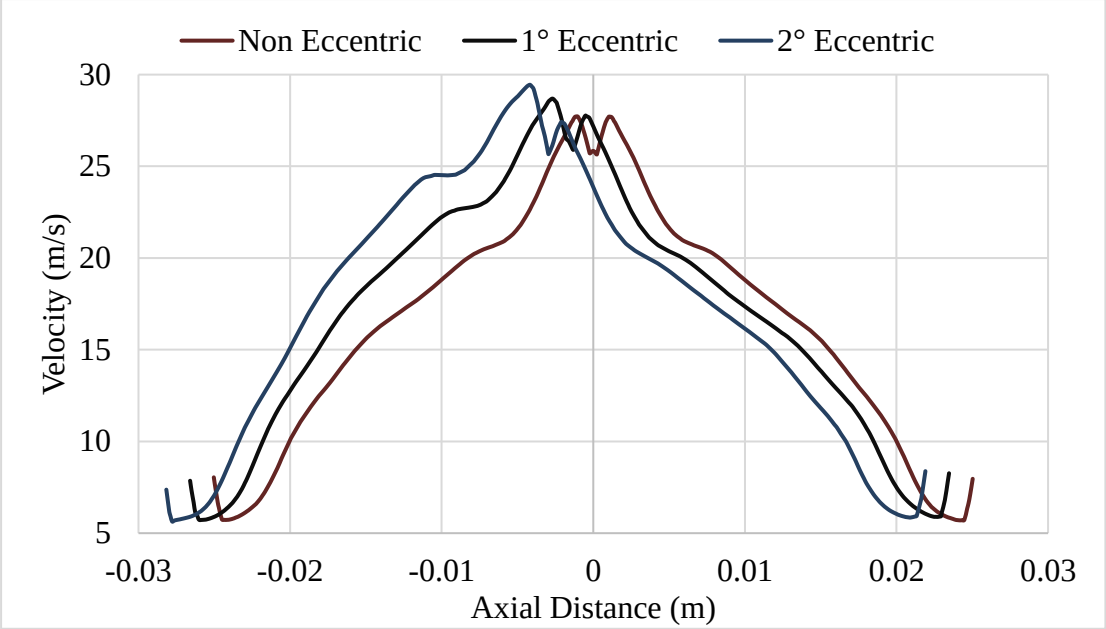

Figure 6.5: Water velocity at bucket mid plane along axial distance

The visualization of pressure distribution at the front side of middle bucket presented at same flow time (at maximum pressure occurring time) for non-eccentric, 1° eccentric and 2° eccentric bucket is shown in Figure 6.6.

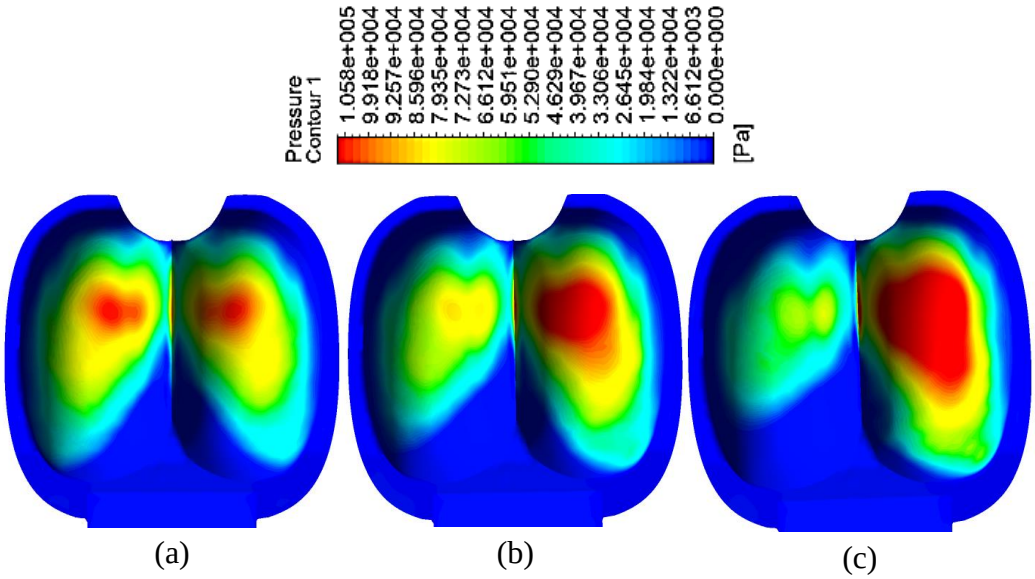

Figure 6.6: Pressure distribution at middle bucket front at maximum pressure occurring flow time for (a) non eccentric (b) 1° eccentric and (c) 2° eccentric bucket

Figure 6.7 shows the maximum pressure values at back side of the middle bucket for successive flow time. The maximum pressure is found to be, 145.905 kPa, 160.059 kPa and 193.466 kPa for non-eccentric, 1° eccentric and 2° eccentric bucket respectively. The maximum pressure at the back side of middle bucket is found to be increasing with the increase in bucket eccentricity.

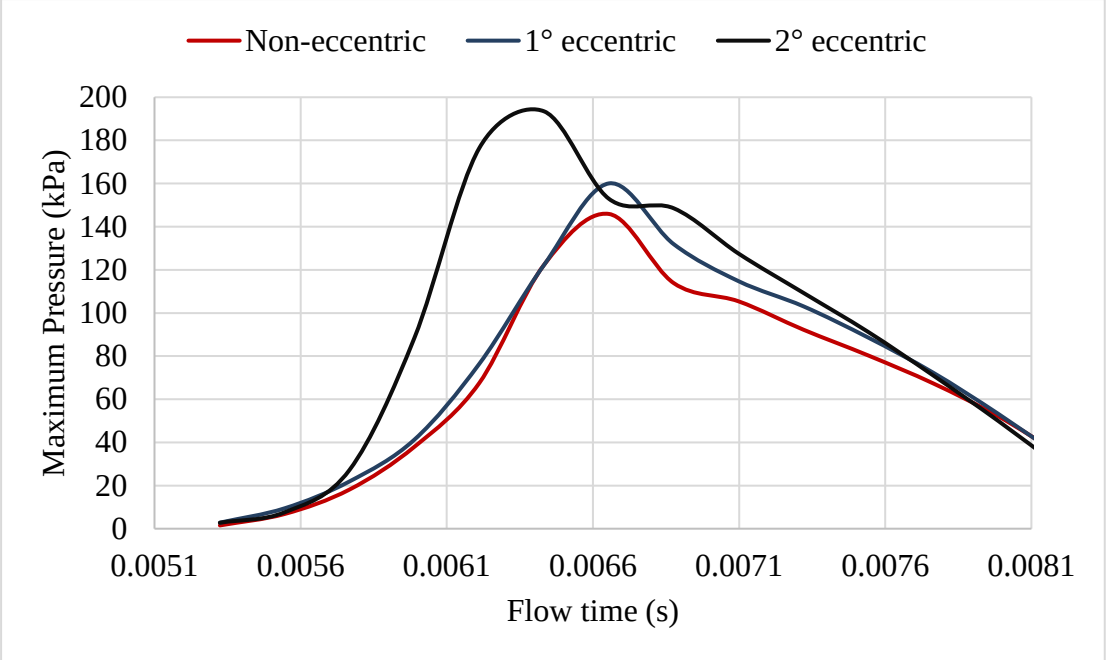

Figure 6.7: Maximum pressure at the back side of middle bucket at successive flow time

Figure 6.8 shows the distance of point at back side of middle bucket, at which the maximum pressure is exerted by water, in the axial direction. The distance is found to be 0 m, 0.00378 m and 0.00599 m for non-eccentric, 1° eccentric and 2° eccentric bucket respectively. The distance of point occurring maximum pressure at the back side of middle bucket is found to be increasing with the increase in bucket eccentricity.

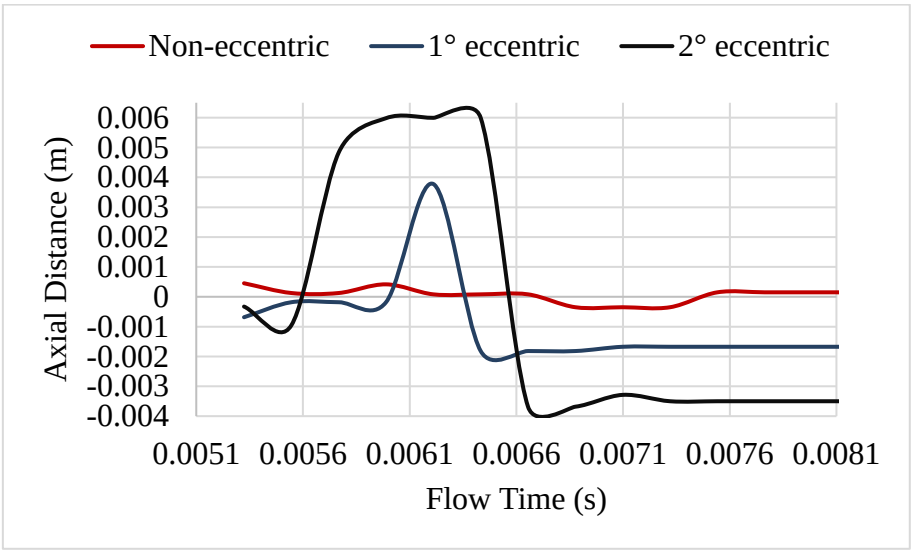

Figure 6.8: Axial distance of maximum pressure point at back side of middle bucket at successive flow time

The visualization of pressure distribution at the back side of middle bucket presented at same flow time (at maximum pressure occurring time) for non-eccentric, 1° eccentric

and 2° eccentric bucket is shown in Figure 6.9. The pressure accumulation on one side of the bucket back makes bucket tips more vulnerable to structural failure.

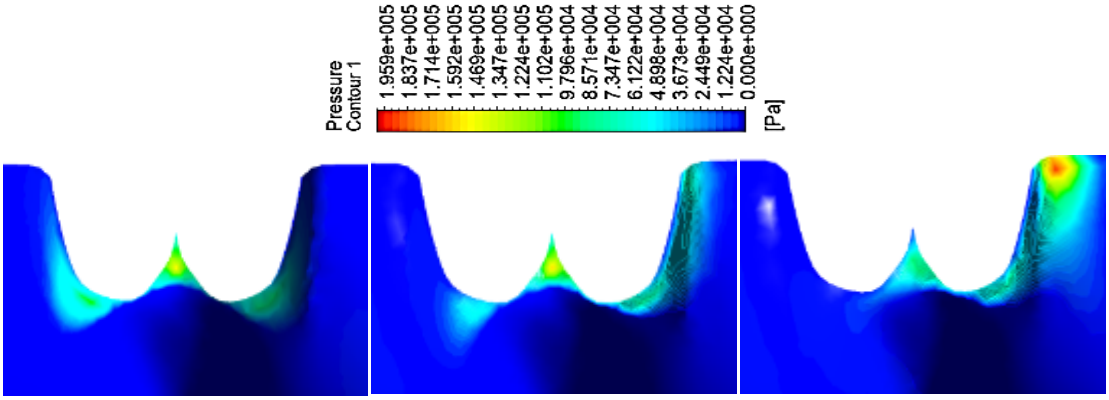

(a) (b) (c)

Figure 6.9: Pressure distribution at middle bucket back at maximum pressure occurring flow time for (a) non eccentric (b) 1° eccentric and (c) 2° eccentric bucket

6.3 Comparison between numerical simulation and mathematical model results

Whenever the experimental work is not feasible to perform due to constraints like cost, time and availability of setup, the CFD user must depend on experiences gained through previous researches, comparison with simpler approximations of problem in the form of analytical expressions but in similar problem or comparisons with the data obtained from the previous literatures which presents the problem and its solution with a very effective and accurate results (Malalasekera & Versteeg, 2007). In this research for the validation, the second option, comparison with analytical solution is performed. Comparison of torque obtained from simulation is done with that obtained from the mathematical calculated value. The mean value of torque at all timesteps was taken for the simulation value. Table 6.2 shows the torque values obtained from simulation and mathematical calculation side by side. The mathematical value was obtained by solving the model developed by substituting the values available.

Table 6.2: Comparison of torque obtained from simulation with mathematical calculation

Axis	Simulation			Mathematical		
	Non-eccentric	1° eccentric	2° eccentric	Non-eccentric	1° eccentric	2° eccentric
X	12.570	12.306	12.148	12.673	12.672	12.671
Y	0.000799	-0.205	-0.372	0	-0.206	-0.396
Z	-0.000859	0.267	0.527	0	0.257	0.515

Figure 6.10 shows the error, expressed in percentage, between torque obtained from simulation and mathematical calculation. The errors are found to be 0.812%, 2.883% and 4.121% for X-axis, 0.079%, 0.205% and 6.017% for Y-axis and 0.086%, 4.207% and 2.411% for Z-axis for non-eccentric, 1° eccentric and 2° eccentric bucket respectively. All the errors are less than 6.017% which conforms the approximation of simulation approach with the mathematical calculation.

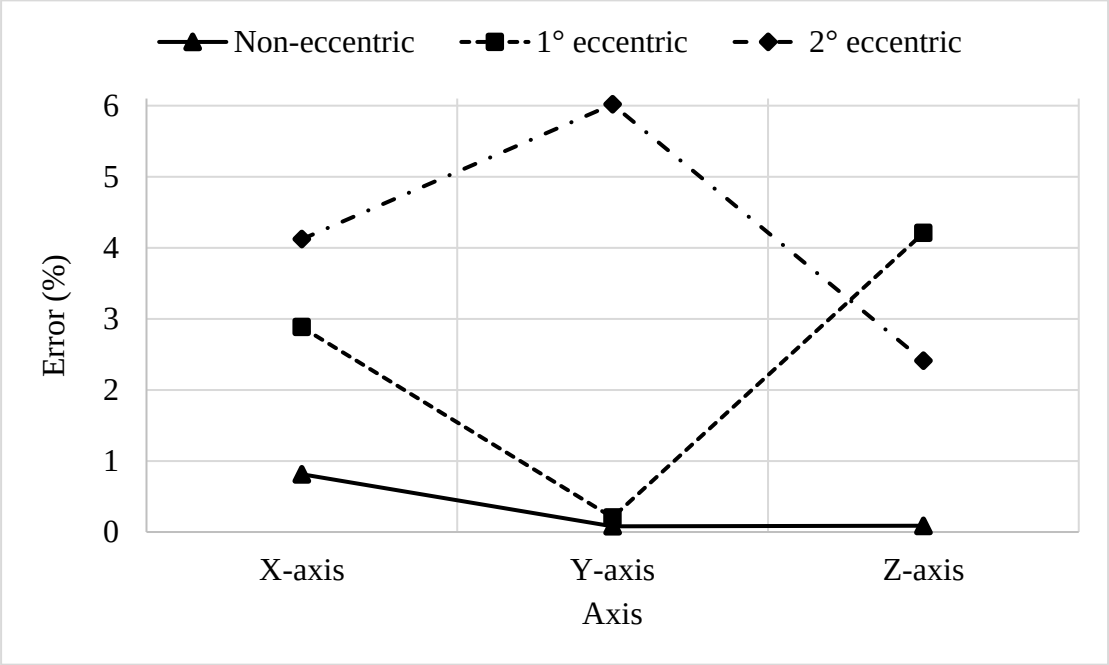

Figure 6.10: Error (%) between the torque value of simulation and mathematical calculation

CHAPTER SEVEN: CONCLUSIONS AND RECOMMENDATIONS

Conclusion

The following conclusions are derived from the research:

- Mathematical model for the calculation of torque generated by eccentric bucket is developed. The equations obtained are solved to find the torque generated. Torque for the non-eccentric, 1° eccentric and 2° eccentric bucket is found to be 12.673Nm, 12.672 Nm and 12.671 Nm about X-axis, 0 Nm, -0.206 Nm and -0.396 Nm about Y-axis and 0 Nm, 0.257 Nm and 0.515 Nm about Z-axis respectively.
- Flow analysis in the Pelton bucket is conducted with the help of computational method. The transient state analysis is conducted for time required for a bucket to rotate through 140 degrees, monitoring the torque generated by buckets. For the modelling of multiphase VOF scheme, flow rate of $5.345 \times 10^{-3} m^3/s$ was maintained at the nozzle outlet with air surrounding the jet area. The velocity distribution revealed lowest velocity at the exit from the bucket. The maximum velocity of water is found at the region near the splitter with the value of 27.724 m/s, 28.688 m/s and 29.444 m/s at the non-eccentric, 1° eccentric and 2° eccentric bucket respectively.
- The pressure distribution at bucket front and back side is obtained from the numerical analysis and studied. The maximum pressure is found to be 107.682 kPa, 125.765 kPa and 137.248 kPa at front side and 145.905 kPa, 160.059 kPa and 193.466 kPa at back side of non-eccentric, 1° eccentric and 2° eccentric bucket respectively. The pressure distribution analysis on back side of the bucket revealed that the maximum pressure occurred at 0 m from the splitter for non-eccentric condition and it goes increasing at 0.00378 m and 0.00599 m from the splitter for 1° and 2° eccentric condition respectively.
- The comparison is done between simulation and mathematical calculated results. For the comparison torque on a single middle bucket is monitored in and later duplicated to get final total torque generated. The mean values of torque obtained from simulation and error is calculated to numerically validate the simulation results by comparing mathematically calculated torque values. The errors are found to be 0.812%, 2.883% and 4.121% for X-axis, 0.079%,

0.205% and 6.017% for Y-axis and 0.086%, 4.207% and 2.411% for Z-axis for non-eccentric, 1° eccentric and 2° eccentric bucket respectively. Since, all the errors are less than 6.017%, the simulation approach followed in this research is in approximation with the theoretical based mathematical model.

Recommendations

- For accurate results it is recommended to conduct flow analysis on a Pelton wheel consisting complete number of buckets and its casing which would provide exact visualization of water interaction with turbine components after exit from the bucket.
- The experimental study by operating actual Pelton wheel with eccentric bucket to conduct flow analysis with the help of high precision cameras and sensors can be conducted to find the actual field results and further verify the results obtained from CFD analysis and mathematical calculations.
- It is recommended to Micro Hydro operators to continuously monitor the bucket eccentricity and conduct a timely re-positioning or changing of used buckets to align the bucket axis uniformly.

REFERENCES

ANSYS, 2011. *CFX Introduction,* Southpointe: ANSYS Inc..

ANSYS, 2011. *CFX-Solver Manager User's Guide.* Southpointe: ANSYS Inc..

ANSYS, 2012. *CFX Solver Theory Guide,* Canonsburg: ANSYS Inc..

ANSYS, 2013. *Meshing User Guide,* 2013: ANSYS Inc..

ANSYS, 2019. *Meshing Solution Ansys.* [Online] Available at: www.ansys.com/products/platform/ansys-meshing#:~:text=Ansys%20Meshing%20Solutions,and%20speed%20of%20the%20simulation.
[Accessed 25 05 2020].

Avellan, F. et al., 2006. Flow in a Pelton Turbine Bucket: Numerical and Experimental Investigations. *Journal of Fluids Engineering,* March, Volume 128, pp. 350-358.

Bansal, R. K., 2010. *A Textbook of Fluid Mechanics and Hydraulic Machines.* Ninth ed. New Delhi: Laxmi Publications (P) Ltd..

Batbeleg, T. & Lee, Y.-H., 2018. *Numerical prediction of the performance of a micro class Pelton turbine.* s.l., s.n.

Brekke, H., 2001. *HYDRAULIC TURBINES: Design, Erection and Operation.* s.l.:s.n.

Chukweneke, J. L., Achebe, C. H., Nwosu, M. C. & Sinebe, J. E., 2014. Analysis and simulation on effect of head and bucket splitter angle on the power output of a pelton turbine. *International Journal of Engineering and Applied Sciences.*

Eggenspieler, G., 2012. *Turbulence Modeling.* s.l.:ANSYS Inc..

Eisenring, M., 1991. *Micro Pelton Turbines.* St. Gallen, Switzerland: Swiss Center for Appropriate Technology.

Gudukeya, L. K., 2017. *Improving the Efficiencies of Pelton Wheel in Micro-Hydro Power Plants.* Bogota, Colombia, s.n., pp. 1089-1100.

Kjølle, A., 2001. *Hydropower in Norway - Mechanical Equipment.* Trondheim: NTNU.

Malalasekera, W. & Versteeg, H. K., 2007. *An Introduction to Computational Fluid Dynamics.* Second ed. Harlow: Pearson Education Ltd..

Menter, F. R., 1994. Two-Equation Eddy-Viscosity Turbulence Models for Engineering Applications. *AIAA Journal*, pp. 1598-1605.

Nasir, B. A., 2013. Design of Micro - Hydro - Electric Power Station. *International Journal of Engineering and Advanced Technology (IJEAT)*, June, 2(5), pp. 39-47.

NEA, 2019. *Nepal Electricity Authority, Generation Directorate*, Kathmandu: Nepal Electricity Authority.

Nigussie, T., Engeda, A. & Dribssa, E. T. R. F. t. C. o. S. S. i. E., 2017. Design, Modeling, and CFD Analysis of a Micro Hydro Pelton. *International Journal of Rotating Machinery*, Volume 2017, pp. 1-17.

Panthee, A., Thapa, B. & Neupane, H. P., 2014. CFD Analysis of Pelton Runner. *International Journal of Scientific and Research Publications.*

Petley, S. M., 2018. *Numerical and Experimental Investigation of Flow in Horizontal Axis Pelton Turbines.* s.l.:Engineering Department, Lancaster University.

Rajput, R. K., 1998. *Hydraulic Machines.* New Delhi: S. Chand.

Riveros, H. G. & Riveros-Rosas, D., 2010. Laminar and turbulent flow in water. *Physics Education*, pp. 288-291.

R. M. H., 2001. *Rainbow Micro Hydro Instruction Manual.* s.l.:Rainbow Power Company Limited.

Sangal, S., Garg, A. & Kumar, D., 2013. Review of Optimal Selection of Turbines for Hydroelectric Projects. *International Journal of Emerging Technology and Advanced Engineering*, March, 3(3), pp. 424-430.

Solemslie, B. W. & Dahlhaug, O. G., 2015. Studying the effects of jet alignment in Pelton units. *Hydropower & Dams*, pp. 78-83.

Thake, J., 2000. *The Micro-hydro Pelton Turbine Manual: Design, manufacture and installation for small-scale hydropower.* s.l.:Intermediate Technology Publications.

White, F. M., 2008. *Fluid Mechanics.* Seventh edition ed. s.l.:Mcgraw Hill.

Xiao, Y. X., Cui, T., Wang, Z. W. & Yan, Z. G., 2012. *Numerical simulation of unsteady free surface flow and dynamic performance for a Pelton turbine.* s.l., IOP Publishing Ltd, pp. 1-8.

Yadav, S., 2011. Some Aspects of Performance Improvement of Pelton Wheel Turbine with Reengineered Blade and Auxiliary Attachments. *International Journal of Scientific & Engineering Research,* September, 2(9), pp. 1-4.

Zhang, Z., 2016. *Pelton Turbines.* Zurich: Springer.

PUBLICATION

Dhungana, S. & Bajracharya, T. R., 2020. *Flow analysis in eccentric bucket of Micro Pelton turbine: Multiphase modelling with transient state condition*. Kathmandu, IOE Graduate Conference.

APPENDIX A: FUNDAMENTAL GOVERNING EQUATIONS

Generally, fluid flow problems for viscous conditions are studied by using three fundamental equations. These equations are based on the conservation of physical systems as explained in this section.

1. Mass conservation equation (continuity equation)

$$\frac{\partial \rho}{\partial t} + \rho \nabla \mathbf{V} = 0 \qquad \text{Equation A-1}$$

2. Momentum conservation equation (Newton's second law)

$$\rho \left(\frac{D\mathbf{V}}{Dt}\right) = \rho g + \nabla \cdot \tau'_{ij} - \nabla p \qquad \text{Equation A-2}$$

When equations of stress are substituted to the equation of momentum for common Newtonian fluids, in the Equation A-2, it gives the Navier-Stokes equation which is fundamental equation of fluid flow in partial form.

3. Energy conservation equation (first law of thermodynamics)

$$\rho \left(\frac{Dh}{Dt}\right) = \frac{Dp}{Dt} + \nabla(k \nabla T) + \Phi \qquad \text{Equation A-3}$$

Where, Φ is known as dissipation function, is given by,

$$\Phi = \tau'_{ij} \left(\frac{u_i}{x_j}\right)$$

the involved viscous stress tensor τ'_{ij} is obtained by,

$$\tau'_{ij} = \mu \left(\frac{\partial u_i}{\partial x_j} + \frac{\partial u_j}{\partial x_i}\right) + \delta_{ij} \lambda (\nabla \cdot \mathbf{V}) \qquad \text{Equation A-4}$$

In this research, the numerical simulation assumes that the fluid involved is incompressible (density is constant). Rewriting the continuity and momentum equations for incompressible ($\rho = constant$) flow, we have,

$$\nabla \cdot \mathbf{V} = 0 \qquad \text{Equation A-5}$$

$$\rho \left(\frac{D\mathbf{V}}{Dt}\right) = \rho g + \mu \nabla^2 \mathbf{V} - \nabla p \qquad \text{Equation A-6}$$

Here the effect of temperature is neglected so, Equation A-3 is not taken into account.

APPENDIX B: RANS TURBULENCE MODELLING

RANS turbulence modelling assumes the fluid in highly unsteady state. In this scenario, any variable $\overline{G}$ is used as the average of parameter G and a parameter which fluctuates, G', is added to it. The expression for the average value is given by,

$$\overline{G} = \frac{1}{T}\int_{t_0}^{t_0+T} G dt \qquad \text{Equation B-1}$$

where the fluctuating period is very small when compared to the parameter T and the average value of the parameter $\overline{G}$ changes with time as flow is considered as turbulent.

$$u = \overline{u} + u' \quad v = \overline{v} + v' \quad w = \overline{w} + w' \quad p = \overline{p} + p' \qquad \text{Equation B-2}$$

$$\overline{u} = \overline{\overline{u} + u'} = \overline{\overline{u}} + 0 \quad \Rightarrow \overline{\overline{u}} = \overline{u} \qquad \text{Equation B-3}$$

Inserting Equations B-2 into A-6 and taking the time-average Equation B-3 of the velocity components u, v, w and pressure p one obtains

$$\rho\left(\frac{D\overline{V}}{Dt}\right) + \rho\left(\frac{\partial}{\partial x_j}\left(\overline{u_i' u_j'}\right)\right) = \rho g + \mu\nabla^2\overline{V} - \nabla\overline{p} \qquad \text{Equation B-4}$$

Which is vector equation of averaged momentum for the incompressible condition and tensor components, comprising various variables are given by the tensor $\overline{u_i' u_j'}$ of inertia of the turbulent flow. When this tensor is rearranged, new equation is obtained from Equation B-4.

$$\rho\left(\frac{D\overline{V}}{Dt}\right) = \rho g + \nabla \cdot \tau_{ij} - \nabla\overline{p} \qquad \text{Equation B-5}$$

Where,

$$\tau_{ij} = \underbrace{\mu\left(\frac{\partial u_i}{\partial x_j} + \frac{\partial u_j}{\partial x_i}\right)}_{Laminar} - \underbrace{\rho\overline{u_i' u_j'}}_{Turbulent}$$

and it can be known that turbulent inertia variables are written as in the form of stresses. Mathematically, it can be understood that the turbulent inertia terms have behavior as

the Newtonian viscous stress when added to another turbulent stress tensor $-\rho\overline{u_i' u_j'}$ (6 new unknowns) gives the total stress of the problem. There are various turbulence model and they have their own systems and processes to find the solution of RANS equations. These approaches are generally differentiated by the number of transport equations as presented in Table B-1.

Table B-1: Extra transport equations needed to solve RANS turbulence model

SN	Number of Transport Equation	Name
1.	Zero	Mixing-length model
2.	One	Turbulent kinetic energy
3.	Two	K-ω, K-ε and SST model
4.	Seven	Reynolds stress models

APPENDIX C: EXPRESSIONS USED IN CFX SETUP

Table C-1: Expressions used in CFX setup to define variables used for the solution

SN	Name	Expression	Description
1.	Head	47.719 [m]	Head
2.	Gravity	9.81 [m s^-2]	Acceleration due to gravity
3.	CoV	0.98	Coefficient of Velocity
4.	InletVel	CoV*sqrt(2*Gravity*Head)	Velocity at the runner inlet or nozzle outlet
5.	Ku	0.45	Speed ratio
6.	RunVel	Ku*sqrt(2*Gravity*Head)	Velocity of runner
7.	PCD	175 [mm]	Pitch Circle Diameter
8.	AngVel	2*RunVel/PCD	Angular Velocity of runner
9.	RPM	AngVel/(2*pi) [min^-1]	Speed of runner
10.	TotalTime	((140*pi)/180)/AngVel	Total time required for snalysis
11.	Data Step	Total Time/70	Time for a single step
12.	DataStep2	DataStep*1.5	Maximum time for a step
13.	InitialDataStep	DataStep	Time at which the simulation is initialized
14.	Output	DataStep	Time at which the outputs from simulations are saved
15.	TorqueMBCx	torque_x@REGION:MBC	Torque at middle bucket about X-axis
16.	TorqueMBCy	torque_y@REGION:MBC	Torque at middle bucket about Y-axis
17.	TorqueMBCz	torque_z@REGION:MBC	Torque at middle bucket about Z-axis

APPENDIX D: MATLAB CODE

```
initial = TorqueVsTime;
tar  = 0.001;
nt = 10;
g = 9.81;
r = 87.5;
Z = 16;
H = 47.719;

c1 = 0.98*sqrt(2*g*H);
u = 0.45*sqrt(2*H*g);
omeg = 1000*(u/r);
rpm = (60*omeg/(2*pi));
f = (omeg*Z)/(2*pi);
dt = 1/f;

T_tem (1,1) = 0;
T_tem (2:size(initial,1)+1,1) = initial(:,3);
T_tem (1,2) = 0;
T_tem (2:size(initial,1)+1,2) = initial(:,2);
clear initial

for i = 2:size(T_tem (:,1),1)
    T_tem (i,3) = T_tem (i,1)-T_tem (i-1,1);
end

mins = min(T_tem (2:end,3));
t_sum = T_tem (end,1);

err  = 1;
ts = 1;
i = size(T_tem (:,1),1);

while err >= tar
    ts = t_sum/i;

    move = round(dt/ts);

    err = abs((dt-ts*move)/ts);

    if ts > 0.5*mins
        err = 1;
    end
    if err >= tar
        i = i + 1;
    else
        break
    end
end
```

```
T(:,1) = T_tem (2,1):ts:(t_sum+(nt*dt));

Tn(:,1) = T_tem (2,1):ts:T_tem (end,1);
Tn(:,2) = spline(T_tem (:,1),T_tem (:,2),Tn(:,1));
plot(Tn(:,1),Tn(:,2));

R = size(Tn,1);
for n = 1:nt
    if n == 1
        T(1:R,n+1) = Tn(:,2);
    else
        T(move*(n-1):move*(n-1)+R-1,n+1) = Tn(:,2);
    end
end

p = find(T(:,n+1)~=0);
p = p(end);
for g = 1:p
    T(g,n+2) = sum(T(g,2:n+1));
end
plot(T(:,1),T(:,12), Tn(:,1),Tn(:,2));
Max=max(T(:,12));

T(p+1:size(T,1),:) = [];

clear Tn n nt p R g T_tem
```

APPENDIX E: RESULTS FROM FLOW ANALYSIS

Table E-1: Pressure contour in middle bucket at different angular positions

Position	Non eccentric	1° eccentric	2° eccentric
76°	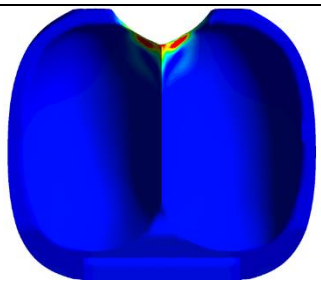	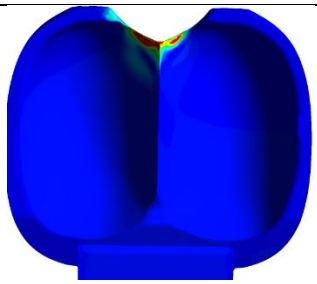	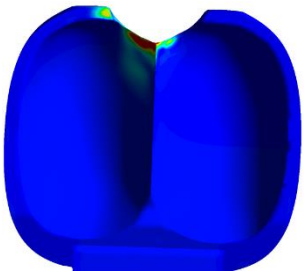
88°	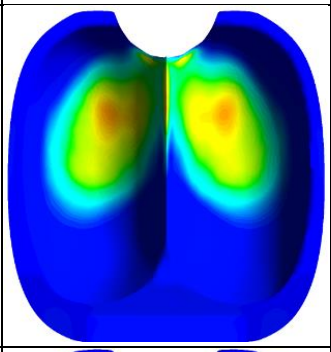	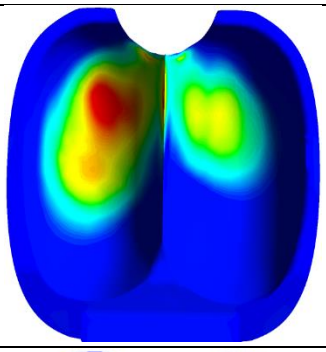	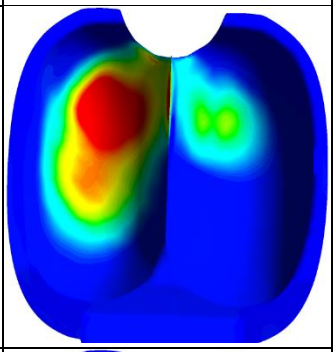
100°	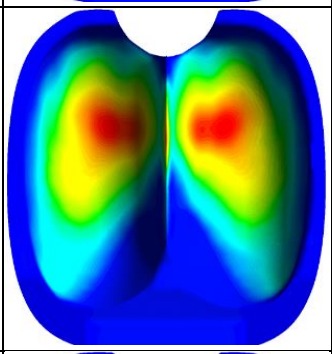	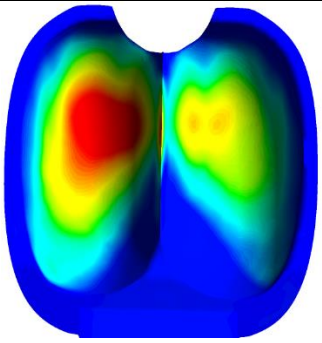	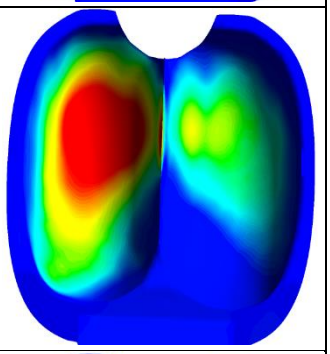
112°	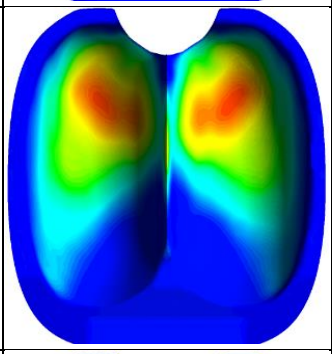	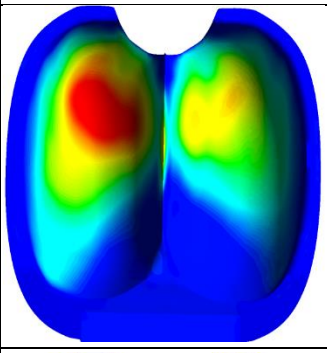	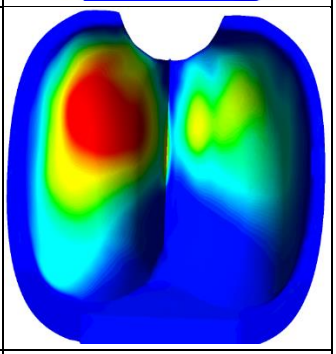
120°	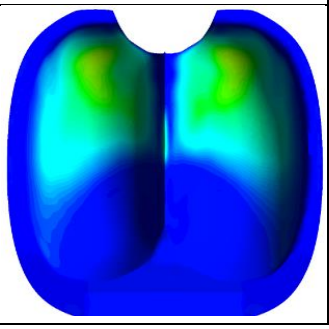	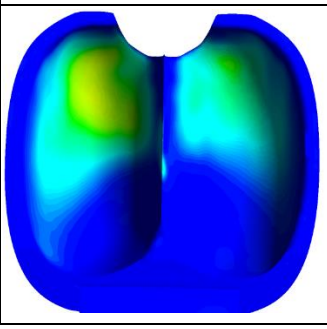	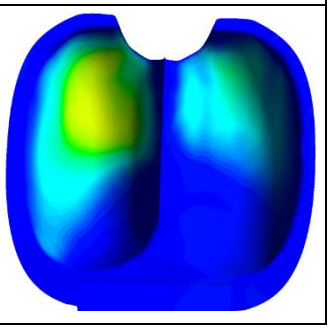

Table E-2: VOF contour at different angular positions

Angular Position	Non eccentric	1° eccentric	2° eccentric
76°	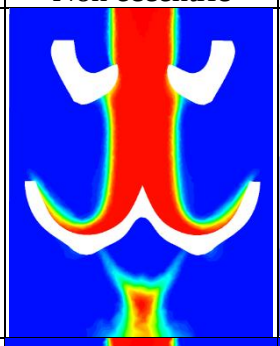	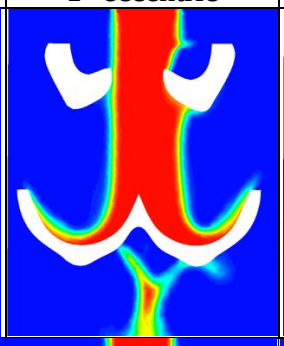	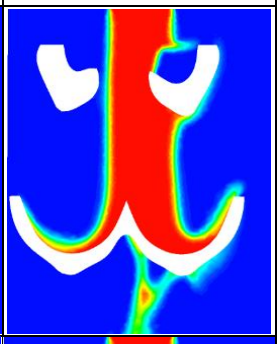
88°	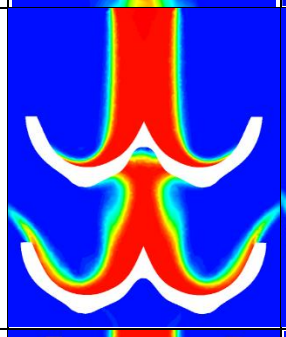	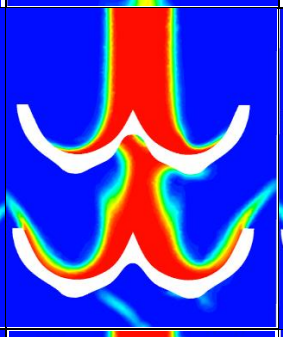	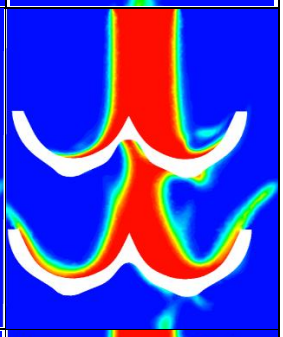
100°	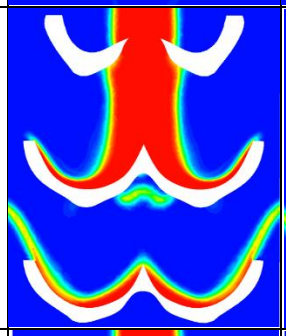	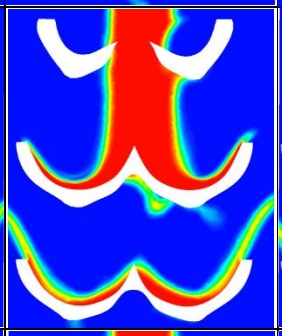	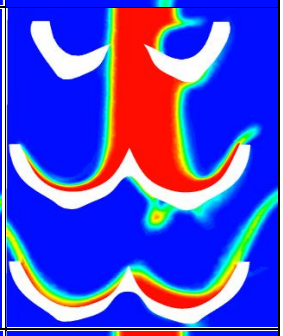
112°	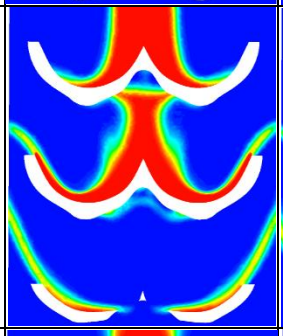	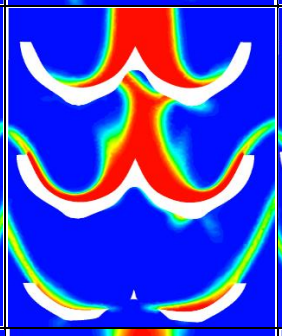	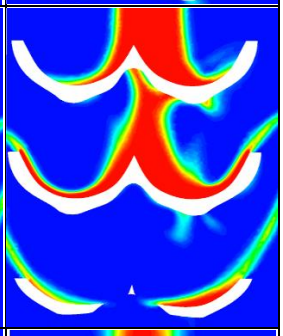
120°	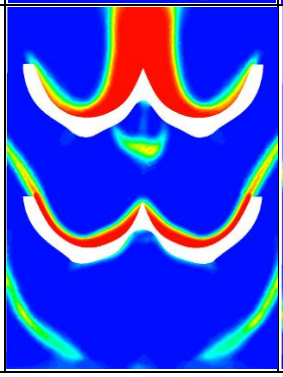	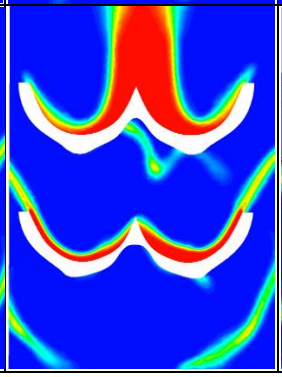	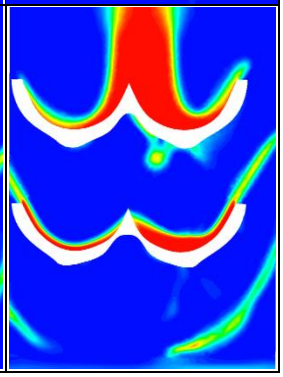

Comparison of torques obtained from numerical simulation and mathematical calculation

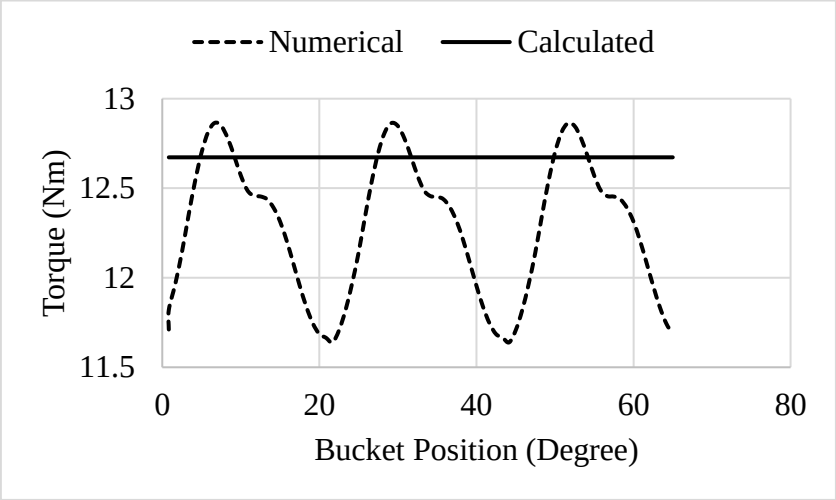

Torque about X-axis with no eccentricity

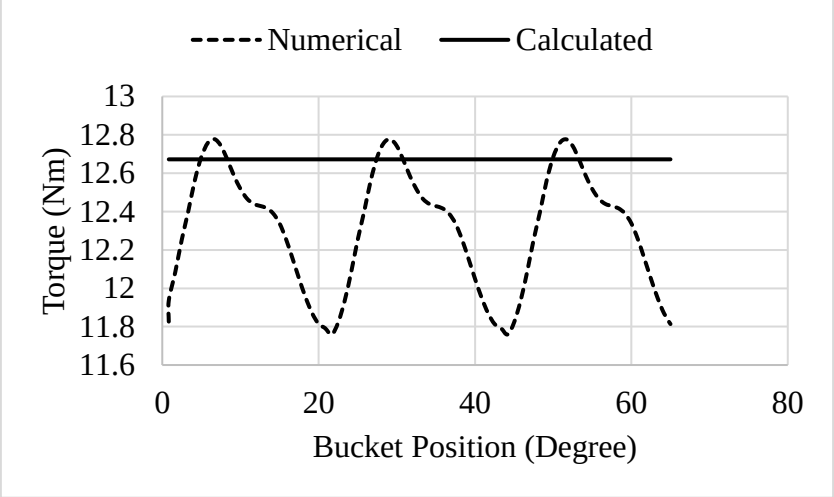

Torque about X-axis with 1° eccentricity

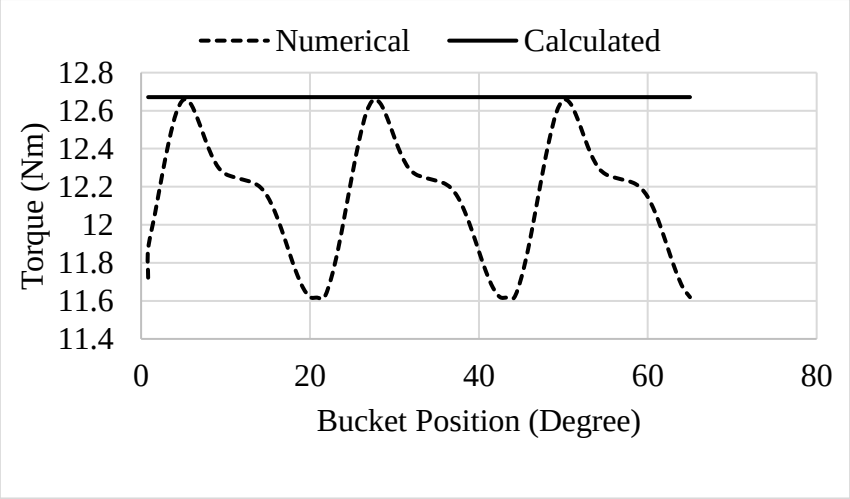

Torque about X-axis with 2° eccentricity

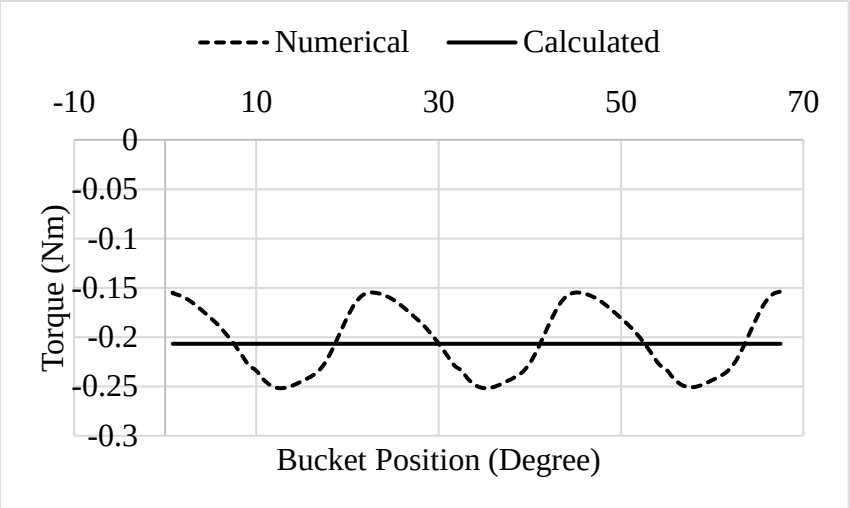

Torque about Y-axis with 1° eccentricity

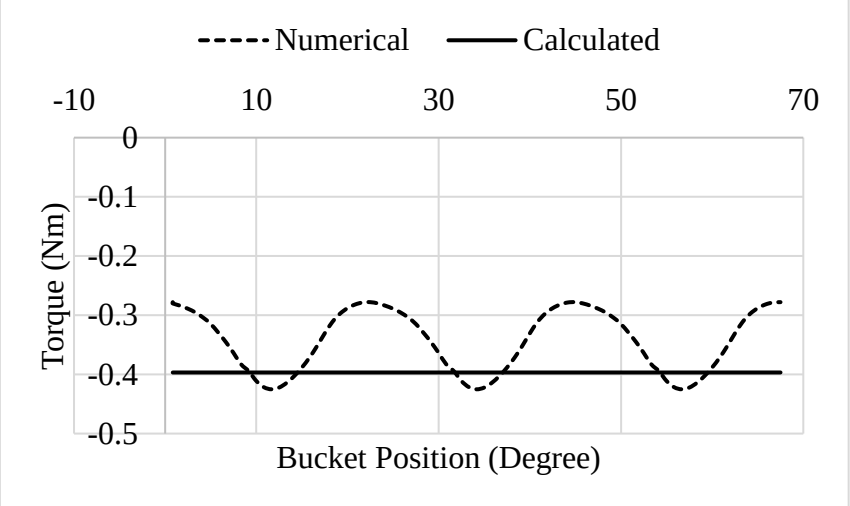

Torque about Y-axis with 2° eccentricity

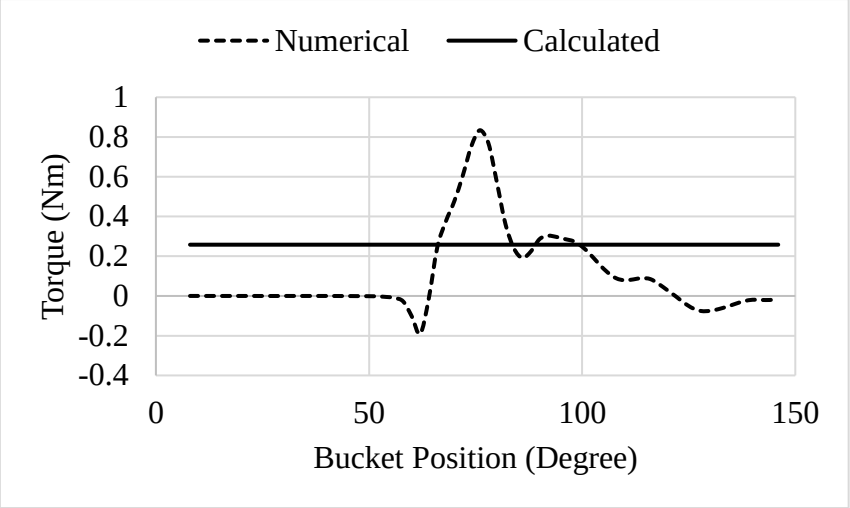

Torque about Z-axis with 1° eccentricity

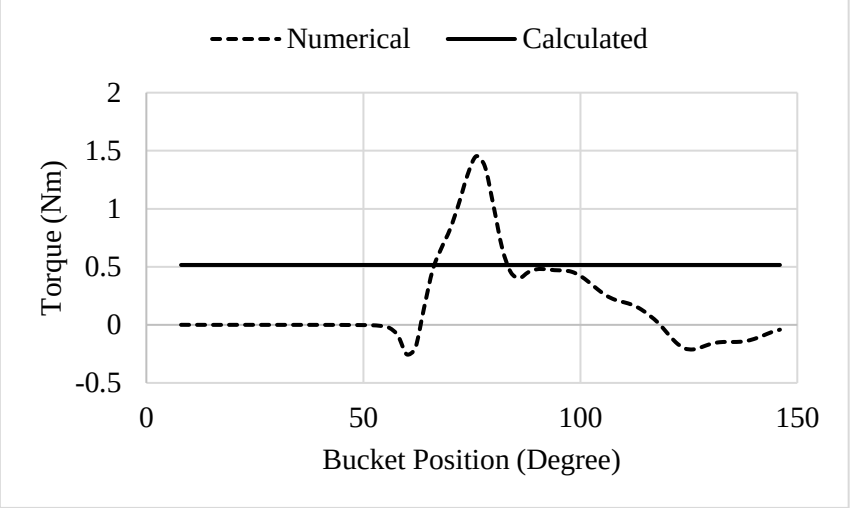

Torque about Z-axis with 2° eccentricity

Results obtained from CFX

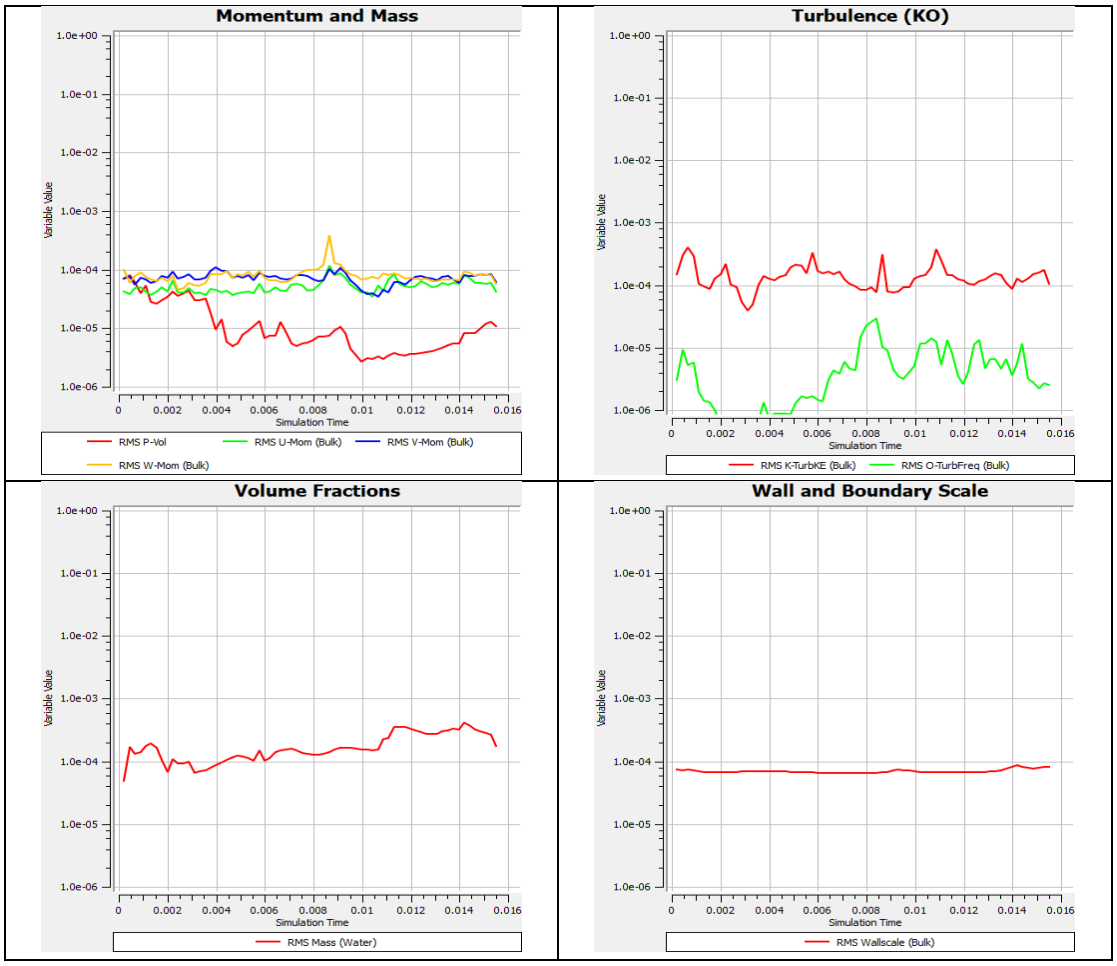

Residuals from CFX Solver Manager for non-eccentric bucket

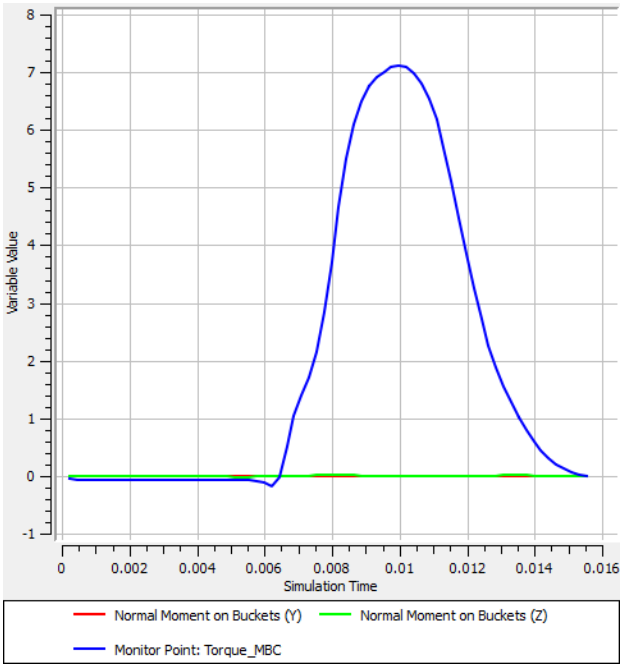

Torque generated for a complete 140° rotation of single bucket for non-eccentric bucket

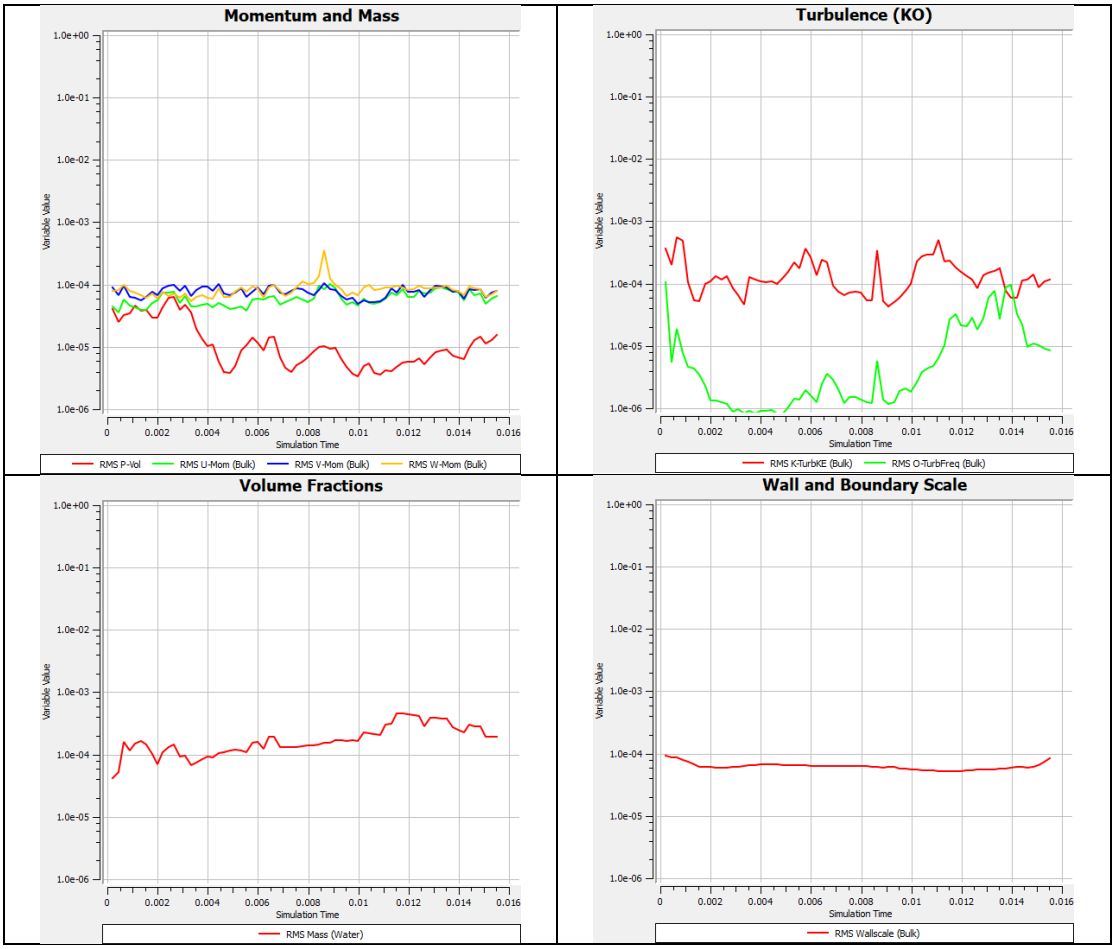

Residuals from CFX Solver Manager for 1° eccentric bucket

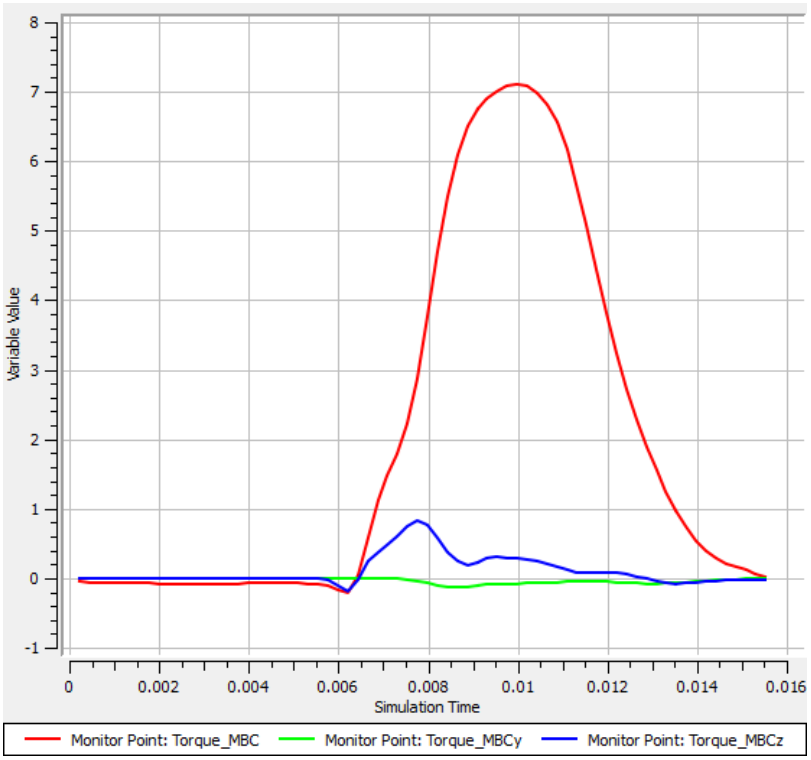

Torque generated for a complete 140° rotation of a single bucket for 1° eccentric bucket

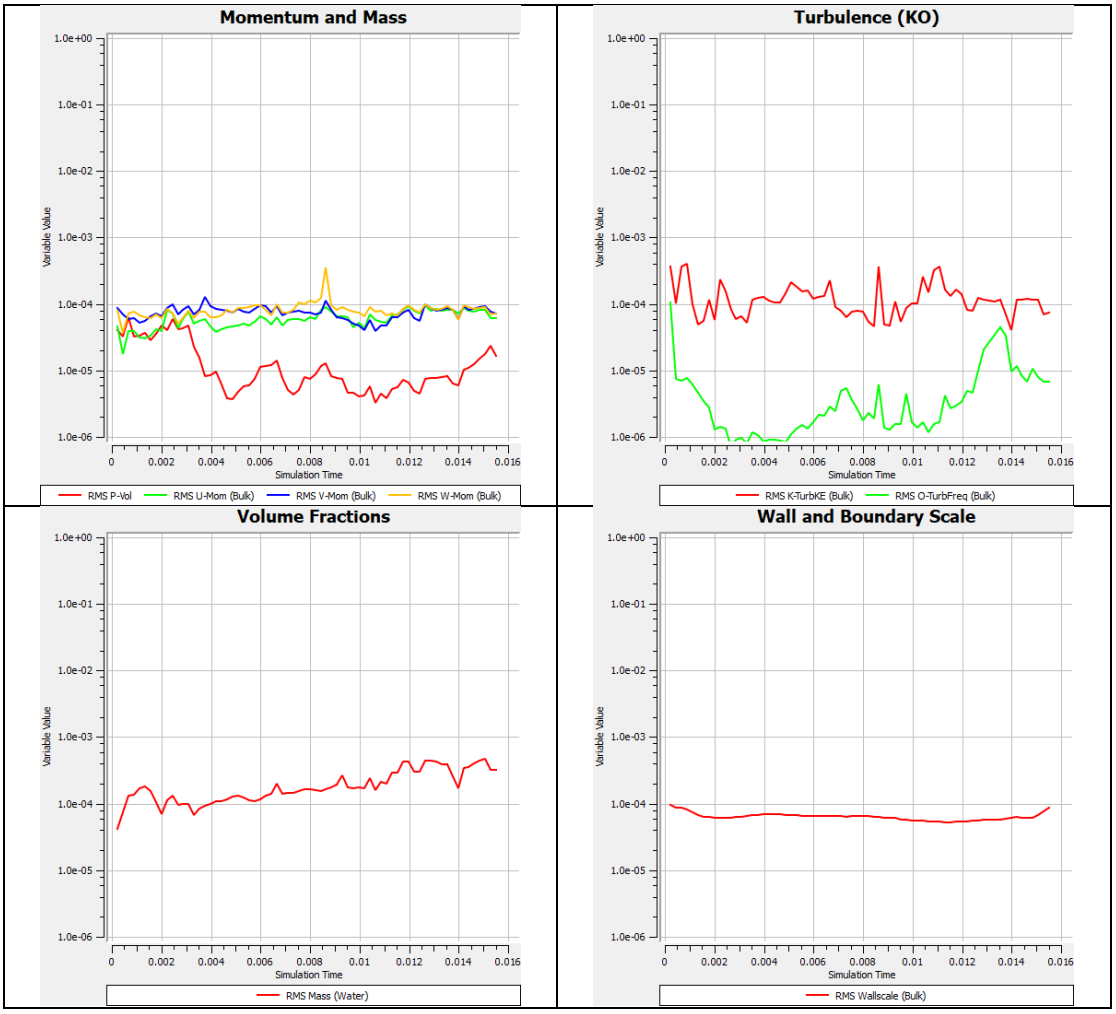

Residuals from CFX Solver Manager for 2° eccentric bucket

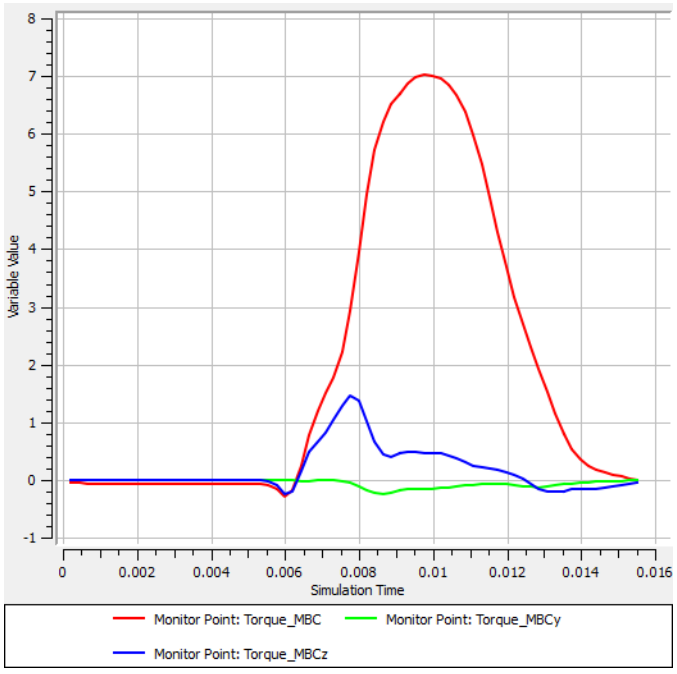

Torque generated for a complete 140° rotation of a single bucket for 2° eccentric bucket

APPENDIX F: ORIGINALITY REPORT

ORIGINALITY REPORT

13%	9%	5%	10%
SIMILARITY INDEX	INTERNET SOURCES	PUBLICATIONS	STUDENT PAPERS

PRIMARY SOURCES

1	core.ac.uk Internet Source	2%
2	Submitted to Seoul National University Student Paper	1%
3	Submitted to University of Technology, Sydney Student Paper	1%
4	Submitted to Higher Education Commission Pakistan Student Paper	<1%
5	Submitted to The British College Student Paper	<1%
6	umpir.ump.edu.my Internet Source	<1%
7	Submitted to Heriot-Watt University Student Paper	<1%
8	Submitted to NCC Education Student Paper	<1%
9	Submitted to Universiti Malaysia Pahang	

	Student Paper	<1%
10	asmedigitalcollection.asme.org Internet Source	<1%
11	Submitted to University of Leeds Student Paper	<1%
12	flipkarma.com Internet Source	<1%
13	Submitted to Blackpool and The Fylde College, Lancashire Student Paper	<1%
14	Submitted to University of Petroleum and Energy Studies Student Paper	<1%
15	www.springerprofessional.de Internet Source	<1%
16	eprints.lancs.ac.uk Internet Source	<1%
17	repository.tudelft.nl Internet Source	<1%
18	Submitted to University of Sheffield Student Paper	<1%
19	Bjørn W. Solemslie, Ole G. Dahlhaug. "A Reference Pelton Turbine—Three-Dimensional	<1%